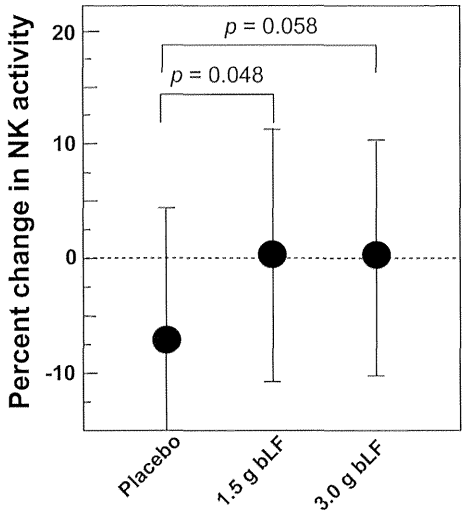

Fig. 8 Effect of bLF on systemic NK cell activity. The change in NK activity in peripheral blood samples measured prior to the beginning and at the end of the trial is shown. There were 33 patients in the placebo group, 37 patients in the 1.5 g bLF group, and 32 patients in the 3.0 g bLF group. The relative change in NK activity in the blood of the trial participants at the end of the one-year trial period was significantly higher in the 1.5 g bLF group compared the placebo group; however, the relative change in the 3.0 g bLF group was not significantly increased compared to the placebo group. This figure is adapted from Fig. 2, Kozu et al. (2009), Effect of Orally Administered Bovine Lactoferrin on the Growth of Adenomatous Colorectal Polyps in a Randomized, Placebo-Controlled Clinical Trial

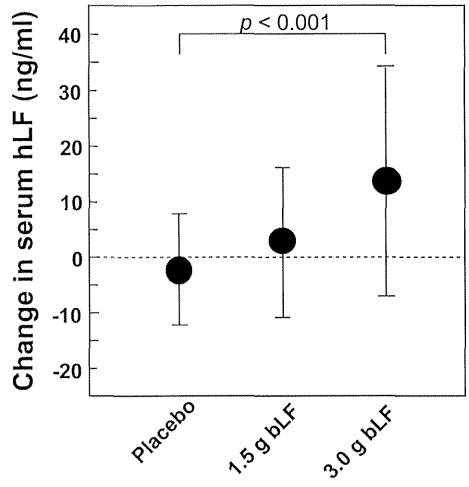

Fig. 9 Effect of bLF on serum hLF levels. The change in hLF levels in serum samples measured prior to the beginning of the trial and at the end of the trial are shown. There were 33 patients in the placebo group, 37 patients in the 1.5 g bLF group, and 32 patients in the 3.0 g bLF group. The levels of serum hLF at the end of the one-year trial period was significantly higher in the 3.0 g bLF group compared the placebo group. This figure is adapted from Fig. 1, Kozu et al. (2009), Effect of Orally Administered Bovine Lactoferrin on the Growth of Adenomatous Colorectal Polyps in a Randomized, Placebo-Controlled Clinical Trial

Polyp associated PMNs, CD66b+, S100A8+ and S100A9+ cells

There was no significant net effect on the presence of PMNs, CD66+ cells, S100A8+ cells or S100A9+ cells in the polyps of trial participants ingesting 3.0 g bLF (data not shown). This result suggests that ingestion of bLF had little effect on the inflammatory potential of the colon mucosa.

Summary and conclusions

The data presented in this report show a good correlation between increased levels of NK cell activity in the blood, increased levels of serum hLF, which reflects systemic neutrophil responsiveness, and regression of colorectal polyps. These data are consistent with a correlation between higher immune system activity and suppression of colorectal polyps.

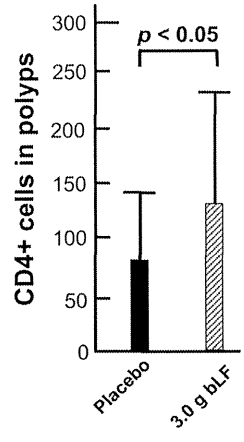

Fig. 10 Effect of bLF on polyp-associated CD4+ cells. At the end of the trial, a final colonoscopic examination was performed. All target polyps were then removed and processed for histological examination. 91 polyps were histologically diagnosed, and the density of CD4+ cells was determined in 37 polyps from the placebo group and 37 polyps from the 3.0 g bLF group. There was a significant increase in CD4+ cells in the polyps from the 3.0 g bLF group compared to the placebo group

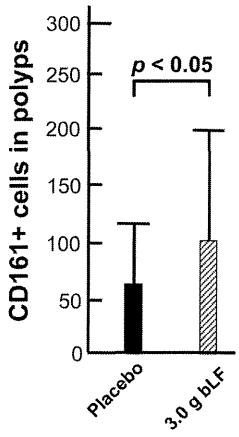

Fig. 11 Effect of bLF on polyp-associated CD161+ cells. At the end of the trial, a final colonoscopic examination was performed. All target polyps were then removed and processed for histological examination. 91 polyps were histologically diagnosed, and the density of CD161+ cells was determined in 37 polyps from the placebo group and 35 polyps from the 3.0 g bLF group. There was a significant increase in CD161+ cells in the polyps from the 3.0 g bLF group compared to the placebo group

Our data also show a good correlation between the presence of CD4+ cells in colorectal polyps and regressing polyps. This finding is consistent with the key role CD4+ cells have in immune system function and is also consistent with a correlation between higher immune system activity and suppression of colorectal polyps. In addition, our data support the proposal that lower inflammatory potential in the colon mucosa, as manifested by decreased numbers of neutrophils and increased numbers of S100A8+ cells, is associated with suppression of colorectal polyps.

Ingestion of bLF caused a possible marginal increase in systemic NK cell activity and a significant increase in serum hLF levels. These findings are consistent with the presence of primed NK cells and neutrophils in the serum. In addition, ingestion of bLF resulted in an increase in the number of CD4+ and NK cells in colorectal polyps. Notably, the colorectal polyps examined in the Tokyo trial persisted throughout the one-year trial period in the patients ingesting 3 g bLF daily, indicating that the polyp-associated CD4+ and NK did not induce an immune response against the polyps. This also consistent with the suggestion that ingestion of bLF primed rather than activated immune effector cells. This premise would predict that ingestion of bLF would not change immune function from OFF to ON, but rather immune function would change from a less responsive state to a more responsive state. Thus, the presence of CD4+ cells and NK cells in polyps without transformed cells would enhance targeting of cells once they acquire a transformed phenotype, thereby decreasing polyp growth. Taken together, our findings are consistent with the proposition that ingestion of bLF suppressed colorectal polyps by enhancing immune system responsiveness.

As previously reported by Kozu et al. (2009), trial participants 63 years old and younger ingesting 3.0 g bLF daily for one year had a statistically significant regression in the growth of colorectal polyps compared with participants ingesting placebo, however, bLF had no significant effect on polyps in participants 64 years old and older. This suggests that while ingestion of bLF resulted in suppression of colorectal polyps, an age related factor affected the trial participants' response to bLF. One possibility is that to generate an effect, bLF must be digested into peptide fragments, and decreased digestive capability in some of the older trial participants resulted in decreased suppression of colorectal polyps in these individuals. Another possibility, is that immune responsiveness was influenced by the inflammatory potential of the colon mucosa, and the inflammatory potential of the colon mucosa of some of the older trial participants was strong enough to counter the effects of bLF.

As noted above, the colorectal polyps examined in the Tokyo trial persisted throughout the one-year trial period in the patients ingesting 3 g bLF daily. A crucial conclusion that can be drawn from this fact is that bLF did not induce an immune response against the polyps. This is a physiologically reasonable and key consideration: The cells in these polyps were mostly pre-cancerous and, consequently, were essentially normal. Lack of an immune response against these cells indicates that the increased responsiveness of immune effector cells in the trial participants ingesting 3.0 g bLF did not result in an autoimmune response. Importantly, in all of the animal and human studies conducted to date, which include chronic administration to animals and daily intake for one year by human patients, ingestion of bLF has been shown to be toxicologically safe.

Acknowledgments This study was partly funded by The Princess Takamarsu Cancer Research Fund and Morinaga Milk Industry Co., Ltd (Tokyo, Japan). We thank Takayuki Akasu

and Takuji Gotoda of the Endoscopic Data-Adjudication Committee, Tadakazu Shimoda, a pathologist, and Takahiro Fujii, an endoscopist (until June 2003). We also thank DIMS institute for technical assistance.

Open Access This article is distributed under the terms of the Creative Commons Attribution License which permits any use, distribution, and reproduction in any medium, provided the original author(s) and the source are credited.

References

Alexander DB, Iigo M, Yamauchi K, Suzui M, Tsuda H (2012) Lactoferrin: an alternative view of its role in human biological fluids. Biochem Cell Biol 90(3):279–306. doi:10.1139/o2012-013

Ambruso DR, Sasada M, Nishiyama H, Kubo A, Komiyama A, Allen RH (1984) Defective bactericidal activity and absence of specific granules in neutrophils from a patient with recurrent bacterial infections. J Clin Immunol 4(1):23–30

Anceriz N, Vandal K, Tessier PA (2007) S100A9 mediates neutrophil adhesion to fibronectin through activation of beta2 integrins. Biochem Biophys Res Commun 354(1):84–89. doi:10.1016/j.bbrc.2006.12.203

Balkwill F, Mantovani A (2001) Inflammation and cancer: back to Virchow? Lancet 357(9255):539–545. doi:10.1016/S0140-6736(00)04046-0

Bhatnagar N, Hong HS, Krishnaswamy JK, Haghikia A, Behrens GM, Schmidt RE, Jacobs R (2010) Cytokine-activated NK cells inhibit PMN apoptosis and preserve their functional capacity. Blood 116(8):1308–1316. doi:10.1182/blood-2010-01-264903

Brown RD, Rickard KA, Kronenberg H (1983) Immunoradiometric assay of plasma lactoferrin. Pathology 15(1):27–31

Brown RD, Yuen E, Rickard KA, Vincent PC, Young G, Kronenberg H (1986) Plasma lactoferrin in patients with neutropenia. Blut 52(5):289–295

Donato R, Cannon BR, Sorci G, Riuzzi F, Hsu K, Weber DJ, Geczy CL (2013) Functions of S100 proteins. Curr Mol Med 13(1):24–57

Freitas M, Porto G, Lima JL, Fernandes E (2008) Isolation and activation of human neutrophils in vitro. The importance of the anticoagulant used during blood collection. Clin Biochem 41(7–8):570–575. doi:10.1016/j.clinbiochem.2007.12.021

Gebhardt C, Nemeth J, Angel P, Hess J (2006) S100A8 and S100A9 in inflammation and cancer. Biochem Pharmacol 72(11):1622–1631. doi:10.1016/j.bcp.2006.05.017

Gessler P, Pretre R, Hohl V, Rousson V, Fischer J, Dahinden C (2004) CXC-chemokine stimulation of neutrophils correlates with plasma levels of myeloperoxidase and lactoferrin and contributes to clinical outcome after pediatric cardiac surgery. Shock 22(6):513–520

Goyette J, Geczy CL (2011) Inflammation-associated S100 proteins: new mechanisms that regulate function. Amino Acids 41(4):821–842. doi:10.1007/s00726-010-0528-0

Hsu K, Passey RJ, Endoh Y, Rahimi F, Youssef P, Yen T, Geczy CL (2005) Regulation of S100A8 by glucocorticoids. J Immunol 174(4):2318–2326

Ichikawa M, Williams R, Wang L, Vogl T, Srikrishna G (2011) S100A8/A9 activate key genes and pathways in colon tumor progression. Mol Cancer Res 9(2):133–148. doi:10.1158/1541-7786.MCR-10-0394

Kozu T, Iinuma G, Ohashi Y, Saito Y, Akasu T, Saito D, Alexander DB, Iigo M, Kakizoe T, Tsuda H (2009) Effect of orally administered bovine lactoferrin on the growth of adenomatous colorectal polyps in a randomized, placebo-controlled clinical trial. Cancer Prev Res (Phila) 2(11):975–983. doi:10.1158/1940-6207.CAPR-08-0208

Lande R, Giacomini E, Grassi T, Remoli ME, Iona E, Miettinen M, Julkunen I, Coccia EM (2003) IFN-alpha beta released by Mycobacterium tuberculosis-infected human dendritic cells induces the expression of CXCL10: selective recruitment of NK and activated T cells. J Immunol 170(3):1174–1182

Lash JA, Coates TD, Lafuze J, Baehner RL, Boxer LA (1983) Plasma lactoferrin reflects granulocyte activation in vivo. Blood 61(5):885–888

Lim SY, Raftery M, Cai H, Hsu K, Yan WX, Hseih HL, Watts RN, Richardson D, Thomas S, Perry M, Geczy CL (2008) S-nitrosylated S100A8: novel anti-inflammatory properties. J Immunol 181(8):5627–5636

Lim SY, Raftery MJ, Goyette J, Hsu K, Geczy CL (2009) Oxidative modifications of S100 proteins: functional regulation by redox. J Leukoc Biol 86(3):577–587. doi:10.1189/jlb.1008608

Megjugorac NJ, Young HA, Amrute SB, Olshalsky SL, Fitzgerald-Bocarsly P (2004) Virally stimulated plasmacytoid dendritic cells produce chemokines and induce migration of T and NK cells. J Leukoc Biol 75(3):504–514. doi:10.1189/jlb.0603291

Mozzanica N, Cattaneo A, Boneschi V, Brambilla L, Melotti E, Finzi AF (1990) Immunohistological evaluation of basal cell carcinoma immunoinfiltrate during intralesional treatment with alpha 2-interferon. Arch Dermatol Res 282(5):311–317

Newton RA, Hogg N (1998) The human S100 protein MRP-14 is a novel activator of the beta 2 integrin Mac-1 on neutrophils. J Immunol 160(3):1427–1435

Queen MM, Ryan RE, Holzer RG, Keller-Peck CR, Jorcyk CL (2005) Breast cancer cells stimulate neutrophils to produce oncostatin M: potential implications for tumor progression. Cancer Res 65(19):8896–8904. doi:10.1158/0008-5472.CAN-05-1734

Roth J, Vogl T, Sunderkotter C, Sorg C (2003) Chemotactic activity of S100A8 and S100A9. J Immunol 171(11):5651

Ryckman C, McColl SR, Vandal K, de Medicis R, Lussier A, Poubelle PE, Tessier PA (2003) Role of S100A8 and S100A9 in neutrophil recruitment in response to monosodium urate monohydrate crystals in the air-pouch model of acute gouty arthritis. Arthritis Rheum 48(8):2310–2320. doi:10.1002/art.11079

Schnekenburger J, Schick V, Kruger B, Manitz MP, Sorg C, Nacken W, Kerkhoff C, Kahlert A, Mayerle J, Domschke W, Lerch MM (2008) The calcium binding protein S100A9 is essential for pancreatic leukocyte infiltration and induces

disruption of cell–cell contacts. J Cell Physiol 216(2):558–567. doi:10.1002/jcp.21433

Simard JC, Girard D, Tessier PA (2010) Induction of neutrophil degranulation by S100A9 via a MAPK-dependent mechanism. J Leukoc Biol 87(5):905–914. doi:10.1189/jlb.1009676

Simard JC, Simon MM, Tessier PA, Girard D (2011) Damage-associated molecular pattern S100A9 increases bactericidal activity of human neutrophils by enhancing phagocytosis. J Immunol 186(6):3622–3631. doi:10.4049/jimmunol.1002956

Sroussi HY, Berline J, Dazin P, Green P, Palefsky JM (2006) S100A8 triggers oxidation-sensitive repulsion of neutrophils. J Dent Res 85(9):829–833

Tsuda H, Kozu T, Iinuma G, Ohashi Y, Saito Y, Saito D, Akasu T, Alexander DB, Futakuchi M,Fukamachi K, Xu J, Kakizoe T, Iigo M (2010) Cancer prevention by bovine lactoferrin: from animal studies to human trial. Biometals 23:399–409. doi:10.1007/s10534-010-9331-3

van den Tol MP, ten Raa S, van Grevenstein WM, van Rossen ME, Jeekel J, van Eijck CH (2007) The post-surgical inflammatory response provokes enhanced tumour recurrence: a crucial role for neutrophils. Digit Surg 24(5):388–394. doi:10.1159/000107781

van der Strate BW, Harmsen MC, The TH, Sprenger HG, de Vries H, Eikelboom MC, Kuipers ME, Meijer DK, Swart PJ (1999) Plasma lactoferrin levels are decreased in end-stage AIDS patients. Viral Immunol 12(3):197–203

Vandal K, Rouleau P, Boivin A, Ryckman C, Talbot M, Tessier PA (2003) Blockade of S100A8 and S100A9 suppresses neutrophil migration in response to lipopolysaccharide. J Immunol 171(5):2602–2609

Wada Y, Yoshida K, Tsutani Y, Shigematsu H, Oeda M, Sanada Y, Suzuki T, Mizuiri H, Hamai Y, Tanabe K, Ukon K, Hihara J (2007) Neutrophil elastase induces cell proliferation and migration by the release of TGF-alpha, PDGF and VEGF in esophageal cell lines. Oncol Rep 17(1):161–167

Wislez M, Antoine M, Rabbe N, Gounant V, Poulot V, Lavole A, Fleury-Feith J, Cadranel J (2007) Neutrophils promote aerogenous spread of lung adenocarcinoma with bronchioloalveolar carcinoma features. Clin Cancer Res 13(12):3518–3527. doi:10.1158/1078-0432.CCR-06-2558

Zhao J, Endoh I, Hsu K, Tedla N, Endoh Y, Geczy CL (2011) S100A8 modulates mast cell function and suppresses eosinophil migration in acute asthma. Antioxid Redox Signal 14(9):1589–1600. doi:10.1089/ars.2010.3583

Cancer Science
Japanese Cancer Association JCA
Open Access

Size- and shape-dependent pleural translocation, deposition, fibrogenesis, and mesothelial proliferation by multiwalled carbon nanotubes

Jiegou Xu,[1,2] David B. Alexander,[1] Mitsuru Futakuchi,[3] Takamasa Numano,[3] Katsumi Fukamachi,[3] Masumi Suzui,[3] Toyonori Omori,[4] Jun Kanno,[5] Akihiko Hirose[6] and Hiroyuki Tsuda[1]

[1]Laboratory of Nanotoxicology Project, Nagoya City University, Nagoya, Japan; [2]Department of Immunology, Anhui Medical University College of Basic Medical Sciences, Hefei, China; [3]Department of Molecular Toxicology, Nagoya City University Graduate School of Medical Sciences, Nagoya; [4]Air Environment Division Environment Management Bureau, Ministry of the Environment, Government of Japan, Tokyo; [5] Divisions of Cellular and Molecular Toxicology; [6] Risk Assessment, National Institute of Health Sciences, Tokyo, Japan

Key words

Fibrosis, mesothelial proliferation, multiwalled carbon nanotubes, parietal pleura, pleural inflammation

Correspondence

Hiroyuki Tsuda, Laboratory of Nanotoxicology Project, Nagoya City University, 3-1 Tanabedohri, Mizuho-ku, Nagoya 467-8603, Japan.
Tel: +81-52-836-3496; Fax: 81-52-836-3497;
E-mail: htsuda@phar.nagoya-cu.ac.jp

Funding Information

Health and Labour Sciences Research Grants of Japan; Princess Takamatsu Cancer Research Fund.

Received January 28, 2014; Revised April 10, 2014; Accepted April 29, 2014

Cancer Sci **105** (2014) 763–769

doi: 10.1111/cas.12437

Multiwalled carbon nanotubes (MWCNT) have a fibrous structure similar to asbestos, raising concern that MWCNT exposure may lead to asbestos-like diseases. Previously we showed that MWCNT translocated from the lung alveoli into the pleural cavity and caused mesothelial proliferation and fibrosis in the visceral pleura. Multiwalled carbon nanotubes were not found in the parietal pleura, the initial site of development of asbestos-caused pleural diseases in humans, probably due to the short exposure period of the study. In the present study, we extended the exposure period to 24 weeks to determine whether the size and shape of MWCNT impact on deposition and lesion development in the pleura and lung. Two different MWCNTs were chosen for this study: a larger sized needle-like MWCNT (MWCNT-L; l = 8 μm, d = 150 nm), and a smaller sized MWCNT (MWCNT-S; l = 3 μm, d = 15 nm), which forms cotton candy-like aggregates. Both MWCNT-L and MWCNT-S suspensions were administered to the rat lung once every 2 weeks for 24 weeks by transtracheal intrapulmonary spraying. It was found that MWCNT-L, but not MWCNT-S, translocated into the pleural cavity, deposited in the parietal pleura, and induced fibrosis and patchy parietal mesothelial proliferation lesions. In addition, MWCNT-L induced stronger inflammatory reactions including increased inflammatory cell number and cytokine/chemokine levels in the pleural cavity lavage than MWCNT-S. In contrast, MWCNT-S induced stronger inflammation and higher 8-hydroxydeoxyguanosine level in the lung tissue than MWCNT-L. These results suggest that MWCNT-L has higher risk of causing asbestos-like pleural lesions relevant to mesothelioma development.

Pleural plaque and malignant mesothelioma are characteristic lesions in asbestos-exposed humans and usually originate from the parietal pleura.[1,2] Properties of asbestos fibers, including dimension, chemical composition, surface reactivity, durability and biopersistence, asbestos deposition-induced oxidative stress and inflammation, and simian virus 40 infection have all been implicated in the pathogenesis of pleural diseases, especially malignant mesothelioma.[3,4]

High concentrations of asbestos fibers have been found in the black spots of the parietal pleura[5] and detected in pleural plaques and malignant mesothelioma[6] in asbestos-exposed patients, suggesting that deposition of asbestos fibers in the parietal pleura is an early event and plays an important role in the pathogenesis of pleural lesions. However, why parietal pleura are the initial and preferential targets of asbestos is not known. According to an explanatory paradigm suggested by Donaldson *et al.*,[7] a fraction of the fibers in the lung are routinely transported into the pleural cavity through unidentified routes. Unlike spherical particles and short fibers, long fibers cannot be cleared effectively through the stomata (small holes in the parietal pleura), resulting in the long fibers being trapped and deposited in the parietal pleura. This deposition causes pro-inflammatory, genotoxic, and mitogenic responses in the deposition sites.[7]

Carbon nanotubes have a fibrous structure with a high aspect ratio. This structural feature, shared with asbestos, raises concern that widespread use of carbon nanotubes may lead to asbestos-like diseases in exposed humans.[8,9] Multiwalled carbon nanotubes (MWCNT) directly injected into the peritoneal cavity or the scrotum in rodents induce mesothelial lesions, including malignant mesothelioma,[10–13] suggesting that inhaled MWCNT may lead to pleural plaque and mesothelioma if fibers enter the pleural cavity. Furthermore, MWCNT administered to the lung has been found to translocate into the pleural cavity and induce inflammation in the pleural cavity and mesothelial cell proliferation in the visceral pleura in mice and rats.[14–16] However, deposition of MWCNT and induction of associated lesions in the parietal pleura have not been reported.

The pleural responses to fibrous particles that deposit in the pleural cavity depend on the size of the particle. Murphy

© 2014 The Authors. Cancer Science published by Wiley Publishing Asia Pty Ltd on behalf of Japanese Cancer Association.
This is an open access article under the terms of the Creative Commons Attribution-NonCommercial-NoDerivs License, which permits use and distribution in any medium, provided the original work is properly cited, the use is non-commercial and no modifications or adaptations are made.

et al.[17] reported that intrapleural injection of long (>15 μm) but not short (<4 μm) MWCNT caused persistent inflammation and fibrosis of the parietal pleura up to 24 weeks post-treatment. Similarly, Schinwald *et al.*[18] reported that injection of silver nanofibers with different lengths into the pleural cavity showed a clear length threshold effect, indicating that fibers longer than 4 μm were pathogenic to the pleura.

The main purpose of the present study was to determine if the size and shape of inhaled MWCNT impact on deposition and associated lesion development in the parietal and visceral pleura. Two different MWCNT were chosen for this study: larger needle-like MWCNTs (MWCNT-L, l = 8 μm, d = 150 nm) and smaller-sized MWCNT (MWCNT-S, l = 3 μm, d = 15 nm) that form cotton candy-like aggregates. We gave relatively high doses (125 μg/rat × 13 doses) of the two MWCNT suspensions over a 24-week period to the rat lung by transtracheal intrapulmonary spraying (TIPS) in order to examine detectable fibers and associated inflammatory and proliferative lesions in the pleura.

Materials and Methods

Animals. Eight-week-old male F344 rats (Charles River, Kanagawa, Japan) were housed on a 12:12 h light:dark cycle and received Oriental MF basal diet (Oriental Yeast, Tokyo, Japan) and water *ad libitum*. The study was conducted according to the Guidelines for the Care and Use of Laboratory Animals of Nagoya City University Medical School (Nagoya, Japan) and the experimental protocol was approved by the Institutional Animal Care and Use Committee (H22M-19).

Preparation of MWCNT suspensions. We used two types of MWCNTs grown in the vapor phase. The larger-sized MWCNTs (MWCNT-L) had a primary mean length of 8 μm and a diameter of 150 nm, and the smaller-sized MWCNTs (MWCNT-S) had a primary mean length of 3 μm and a diameter of 15 nm. Five milligrams of MWCNT-L or MWCNT-S were suspended in 20 mL saline containing 0.5% Pluronic F68 (PF68, non-ionic, biocompatible amphiphilic block copolymers; Sigma-Aldrich, St. Louis, MO, USA) and homogenized for 1 min four times at 3000 rpm in a Polytron PT1600E benchtop homogenizer (Kinematika, Littau, Switzerland). The suspensions were sonicated for 30 min shortly before use to minimize aggregation. The concentration of MWCNTs was 250 μg/mL. The lengths of MWCNT-L in the suspensions were determined using a digital map meter (Comcurve-9 Junior; Koizumi Sokki, Nigata, Japan) on SEM photographs. Characterization of MWCNT including shape, elemental analysis, and size distribution is shown in Figure S1.

Transtracheal intrapulmonary spraying of MWCNTs into the lung and pleural cavity lavage. Spraying of MWCNT suspensions into the lung and pleural cavity lavage (PCL) were carried out as previously described.[15,19] Ten-week-old male Fisher 344 rats were divided into four groups of six animals each. Group 1 did not receive any treatment, and Groups 2, 3, and 4 were given 0.5 mL saline containing 0.5% PF68 or 250 μg/mL MWCNT-L or MWCNT-S suspensions by TIPS under anesthesia by isoflurane once every 2 weeks, 13 times over a 24-week period. The total amount of the MWCNT fibers given to Groups 3 and 4 was 13 × 0.125 = 1.625 mg/rat. Twenty-four hours after the last TIPS, the rats were placed under deep isoflurane anesthesia and PCL was carried out. The rats were then killed by exsanguination from the inferior vena cava. The left lung was frozen in liquid nitrogen for biochemical analysis, and the right lung, as well as other major organs and lymph nodes, were processed for histological examination.

Light microscopy, polarized light microscopy, and SEM. The MWCNT fibers in H&E stained slides of lung tissue, PCL cell pellets, and chest wall sections were observed with polarized light microscopy (PLM, BX51N-31P-O; Olympus, Tokyo, Japan) at ×1000 magnification. The exact localization of the illuminated fibers was confirmed in the same H&E stained sections after removing the polarizing filter.

For SEM, H&E stained slides were immersed in xylene for 2–3 days to remove the cover glass, immersed in 100% ethanol for 10 min to remove the xylene, and air-dried for 2 h at room temperature. The slides were then coated with platinum for viewing the MWCNT fibers by SEM (Model S-4700 Field Emission Scanning Electronic Microscope; Hitachi High Technologies, Tokyo, Japan) at 5–10 kV.

Azan–Mallory staining and measurement of the thickness of the parietal and visceral pleura. To clearly visualize collagen fibers in the lung and the pleura, Azan–Mallory staining was carried out using Azan staining reagents (Muto Pure Chemicals, Tokyo, Japan). The thickness of the pleura was measured on the basis of the Azan–Mallory stained sections (Fig. S2). For the rats treated with MWCNT-L, only the parietal and visceral pleural regions with observed MWCNT-L fibers by PLM were measured. Because obvious thickening of the pleura was not observed in the rats treated with PF68 or MWCNT-S, six pleural regions in each parietal and visceral pleura of each rat were randomly selected for measurement.

Analysis of inflammatory reaction in the pleural cavity. Cells in the lavage fluid were counted using a hemocytometer (Erma, Tokyo, Japan), and the cellular fraction was then isolated by centrifugation at 200g for 5 min at 4°C. To make cell pellets, cells collected from three rats were combined (generating a total of two cell pellets per group) and resuspended in 0.2 mL of 1% sodium alginate (Sigma-Aldrich) by pipetting. The suspension was then solidified by addition of one drop of 1 M $CaCl_2$. The cell pellets were fixed in 4% paraformaldehyde and processed for histological examination. Total protein in the supernatants of each of the lavage fluids was determined using the Pierce BCA Protein Assay Kit (Thermo Fisher Scientific, Rockford, IL, USA). Cytokines and chemokines were analyzed as described below.

Analysis of cytokines and chemokines by Multiplex Suspension Array. Approximately 100 mg of the left lung tissues was rinsed with cold PBS three times and homogenized in 1 mL T-PER Tissue Protein Extraction Reagent (Pierce, Rockford, IL, USA), containing 1% (v/v) proteinase inhibitor cocktail (Sigma-Aldrich). The homogenates were clarified by centrifugation at 10 000 g for 5 min at 4°C. Protein content was measured as described above. The levels of 20 cytokines and chemokines (interleukin [IL]-1α, IL-1β, IL-2, IL-4, IL-6, IL-12 [p70], IL-17, IL-18, granulocyte/macrophage colony-stimulating factors [GM-CSF], granulocyte colony-stimulating factor [G-CSF], tumor necrosis factor [TNF]-α, γ-interferon, monocyte chemotactic protein [MCP]1, macrophage inflammatory protein [MIP]1α, MIP2, interferon gamma-induced protein [IP]-10, regulated on activation, normal T cell expressed and secreted [RANTES], growth related oncogene/ keratinocyte-derived cytokine [GRO/KC], vascular endothelial growth factor [VEGF], and epidermal growth factor [EGF]) in the lung tissue extracts and in the supernatants of the lavage fluids were measured by the Multiplex MAP Rat Cytokine/Chemokines Magnetic Bead Panel (Filgen, Nagoya, Japan).

Immunohistochemistry. CD68, proliferating cell nuclear antigen (PCNA), and mesothelin/Erc were detected using anti-rat CD68 antibodies (BMA Biomedicals, Augst, Switzerland), anti-

© 2014 The Authors. Cancer Science published by Wiley Publishing Asia Pty Ltd on behalf of Japanese Cancer Association.

PCNA mAbs (Clone PC10; Dako Japan, Tokyo, Japan) and anti-rat C-ERC/mesothelin polyclonal antibodies (Immuno-Biological Laboratories, Gunma, Japan). The CD68, PCNA, and C-ERC/mesothelin antibodies were diluted 1:100, 1:200, and 1:1000, respectively, in blocking solution and applied to deparaffinized slides, and the slides were incubated at 4°C overnight. The slides were then incubated for 1 h with biotinylated species-specific secondary antibodies diluted 1:500 (Vector Laboratories, Burlingame, CA, USA) and visualized using avidin-conjugated HRP complex (ABC kit; Vector Laboratories).

Statistical analysis. Statistical analysis was carried out using ANOVA. Statistical significance was analyzed using two-tailed Student's *t*-test. A *P*-value of <0.05 was considered to be significant.

Results

Deposition of MWCNT-L in the pleura. Observation of the pleural tissue sections with PLM and SEM indicated that MWCNT-L deposited in the parietal pleura in four out of six rats, most of the fibers being located in fibrotic parietal pleura, with a few piercing and penetrating into the parietal mesothelium (Fig. 1a–c); MWCNT-L was also found in the visceral pleura (Fig. 1d–f).

Smaller sized MWCNT did not cause polarization and consequently were not detected by PLM (Fig. 1h,k); therefore, observation of MWCNT-S was made mainly by SEM. The MWCNT-S were not found in either the parietal (Fig. 1g–i) or visceral (Fig. 1j) pleura and were often found phagocytosed in alveolar macrophages close to the visceral pleura (Fig. 1j–l).

Fibrosis and mesothelial proliferation in the pleura. Deposition of MWCNT-L in the parietal and visceral pleura was preferentially localized in thickened fibrotic lesions (Fig. 1a,d). Azan–Mallory staining indicated that the thickened lesions were composed of collagen fibers (Fig. 2a). The thickness of the parietal and visceral pleura with deposition of MWCNT-L was 28.75 ± 10.43 μm and 18.92 ± 10.13 μm, respectively, both lesions showing a significant increase compared to those in the rats treated with MWCNT-S (7.28 ± 4.37 μm and 6.16 ± 2.05 μm) or with the dispersing agent, PF68, alone (7.16 ± 4.95 μm and 4.57 ± 1.23 μm; Fig. 2b). An increase in the thickness of the visceral pleura of the rats treated with MWCNT-S compared with the PF68-treated rats was also observed (Fig. 2b).

Neoplastic development was not found in the parietal or visceral pleura of either the MWCNT-L or MWCNT-S groups; however, in the MWCNT-L group, patchy foci of mesothelial cell proliferation were observed in the parietal pleura (Fig. 3a) and PCNA indices were significantly increased in both parietal and visceral mesothelium. The PCNA indices of the MWCNT-S group were comparable to those of the PF68 treated rats (Fig. 3b).

Translocation of MWCNT-L into the pleural cavity. In the cell pellets of the PCL, MWCNT-L was found with both PLM and SEM observations. Larger sized MWCNT fibers were observed mainly within and/or attached to the cell surface of macrophages (Fig. 4a). The ratio of the MWCNT-L containing macrophages to the total cell count was approximately 1:1800 and the average length of MWCNT-L was 6.23 ± 4.11 μm (data not shown). Smaller sized MWCNT could not be detected (Fig. 4a).

Inflammation in the pleural cavity. Both MWCNT-L and MWCNT-S treatments caused inflammatory reactions in the

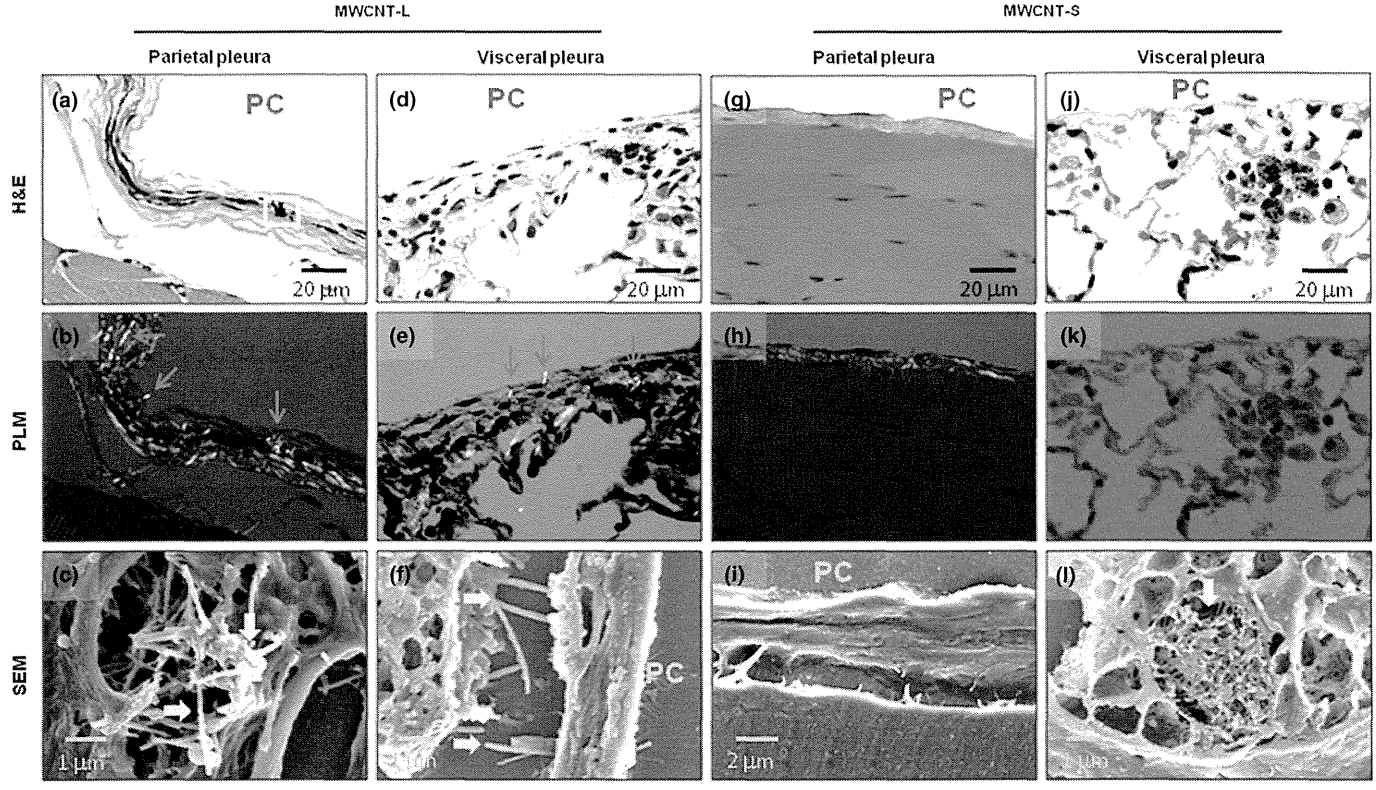

Fig. 1. Evidence of multiwalled carbon nanotube (MWCNT) fibers in the pleura. Existence of MWCNT fibers in the parietal (a–c, g–i) and visceral (d–f, j–l) pleura of rats treated with larger sized MWCNT (MWCNT-L; *l* = 8 μm, *d* = 150 nm) (a–f) or smaller sized MWCNT (MWCNT-S; *l* = 3 μm, *d* = 15 nm) (g–l) was examined by polarized light microscopy (PLM) (d, e, h, k) and SEM (c, f, i, l). The area in (a) denoted by the square was subjected to SEM observation, shown in (c). Arrows indicate MWCNT fibers. PC, pleural cavity.

© 2014 The Authors. Cancer Science published by Wiley Publishing Asia Pty Ltd on behalf of Japanese Cancer Association.

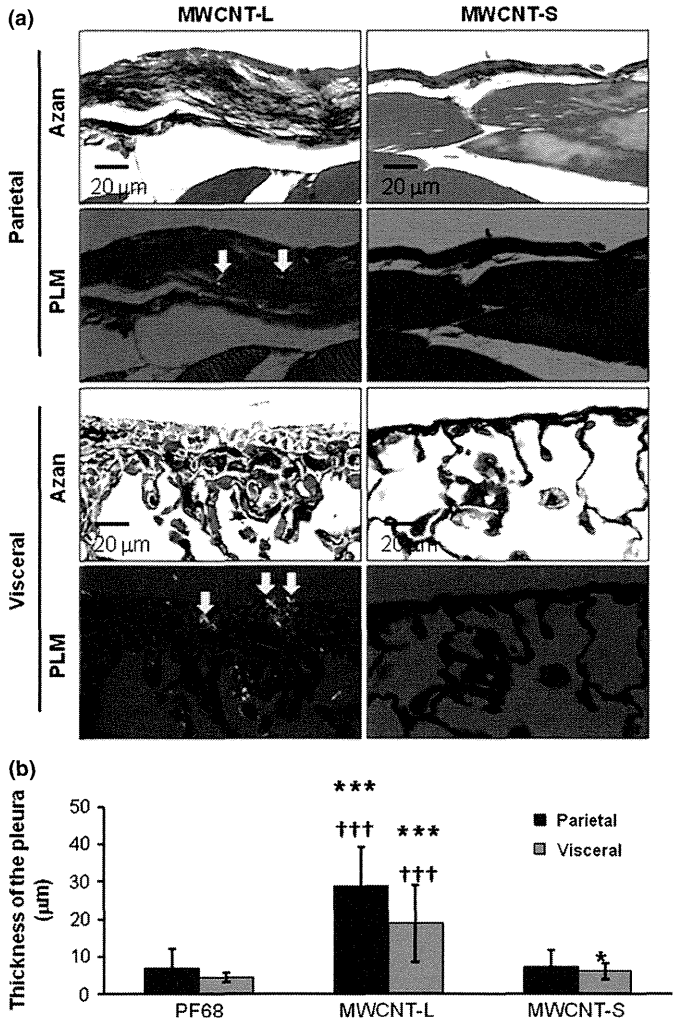

Fig. 2. Azan–Mallory (Azan) staining and thickness of the parietal and visceral pleura. (a) Azan–Mallory staining images and polarized light microscopy (PLM) images of the parietal and visceral pleura in rats sprayed with larger sized multiwalled carbon nanotubes (MWCNT-L; l = 8 μm, d = 150 nm) or smaller sized MWCNT (MWCNT-S; l = 3 μm, d = 15 nm). (b) Quantification of the thickness of the parietal and visceral pleura of rats treated with Pluronic F68 (PF68), MWCNT-L, or MWCNT-S on the basis of Azan–Mallory stained images. *P < 0.05 versus PF68; ***P < 0.001 versus PF68; $^{\dagger\dagger\dagger}P$ < 0.001 MWCNT-L versus MWCNT-S by two-tailed Student's t-test. Arrows indicate MWCNT fibers.

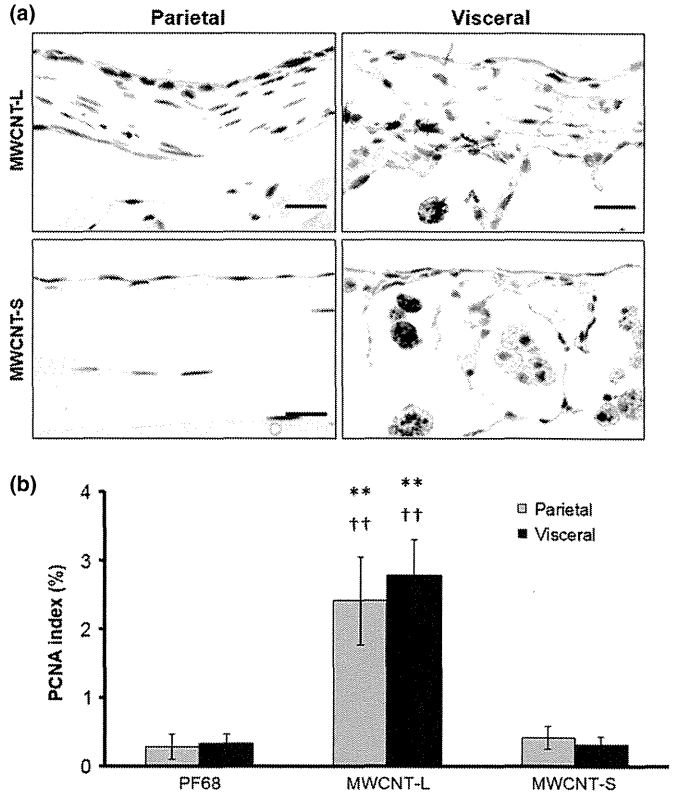

Fig. 3. Cell proliferation of the parietal and visceral mesothelium. (a) Representative proliferating cell nuclear antigen (PCNA) immunostained images of the parietal and visceral pleural regions of rats treated with larger sized multiwalled carbon nanotubes (MWCNT-L; l = 8 μm, d = 150 nm) or smaller sized MWCNT (MWCNT-S; l = 3 μm, d = 15 nm). (b) PCNA indices (percentages of PCNA positive mesothelial cells in total mesothelial cells). Scale bar = 20 μm. **P < 0.01 versus Pluronic F68 (PF68); $^{\dagger\dagger}P$ < 0.01 MWCNT-L versus MWCNT-S.

pleural cavity. In the PCL, the total cell number, composed mostly of macrophages, neutrophils, eosinophils, and lymphocytes, in the MWCNT-L and MWCNT-S treated groups was significantly increased compared with the PF68 group. The PCL cell number in the MWCNT-L group was significantly greater than in the MWCNT-S group (Fig. 4b). A similar pattern was observed for the ratio of cells positive for CD-68, a macrophage/monocyte marker (Fig. 4c). The ratios of cells in the PCL pellets positive for mesothelin/Erc, a mesothelial cell marker, were approximately 1%, indicating that the increased cell number in the pleural cavity of the rats treated with MWCNT-L and MWCNT-S was caused by inflammatory cell effusion, not by mesothelial cell shedding from the mesothelium. Treatment with MWCNT-L also caused an increase in the total protein level of the cell-free PCL (Fig. 4d). Analysis of 20 cytokines and chemokines by Multiplex Suspension Array indicated that the levels of IP-10, RANTES, IL-2, and IL-18 were significantly higher in the MWCNT-L group than the MWCNT-S group (Table 1).

Toxicological responses in the lung. In the lung tissue, both MWCNT-L and MWCNT-S treatments induced small granulation foci and scattered infiltration of macrophages in the alveoli (Fig. S3A,B). Alveolar neoplastic proliferation was not found. The number of alveolar macrophages was higher in the MWCNT-S group than in the MWCNT-L group. We were unable to quantitatively analyze the alveolar macrophage number, because most of the alveolar macrophages induced by MWCNT-S were degenerative or necrotic. Most of the MWCNT-L fibers were found within alveolar macrophages (Fig. S3C), with a few penetrating the alveolar epithelium (Fig. S3D), whereas MWCNT-S fibers were observed in alveolar macrophages, but not in the alveolar epithelium (Fig. S3E). Multiplex Suspension Array analysis of 20 cytokines and chemokines in the lung tissue indicated that the levels of MIP1α, MIP2, MCP1, IP10, IL-1β, IL-18, and VEGF were significantly higher in the MWCNT-S group than in the MWCNT-L group; the values of GRO/KC and IL-1α were elevated in both the MWCNT-L and MWCNT-S treated groups without an intergroup difference. The level of RANTES was significantly higher in the MWCNT-L group than the MWCNT-S group, and the other 10 cytokines were compara-

© 2014 The Authors. Cancer Science published by Wiley Publishing Asia Pty Ltd on behalf of Japanese Cancer Association.

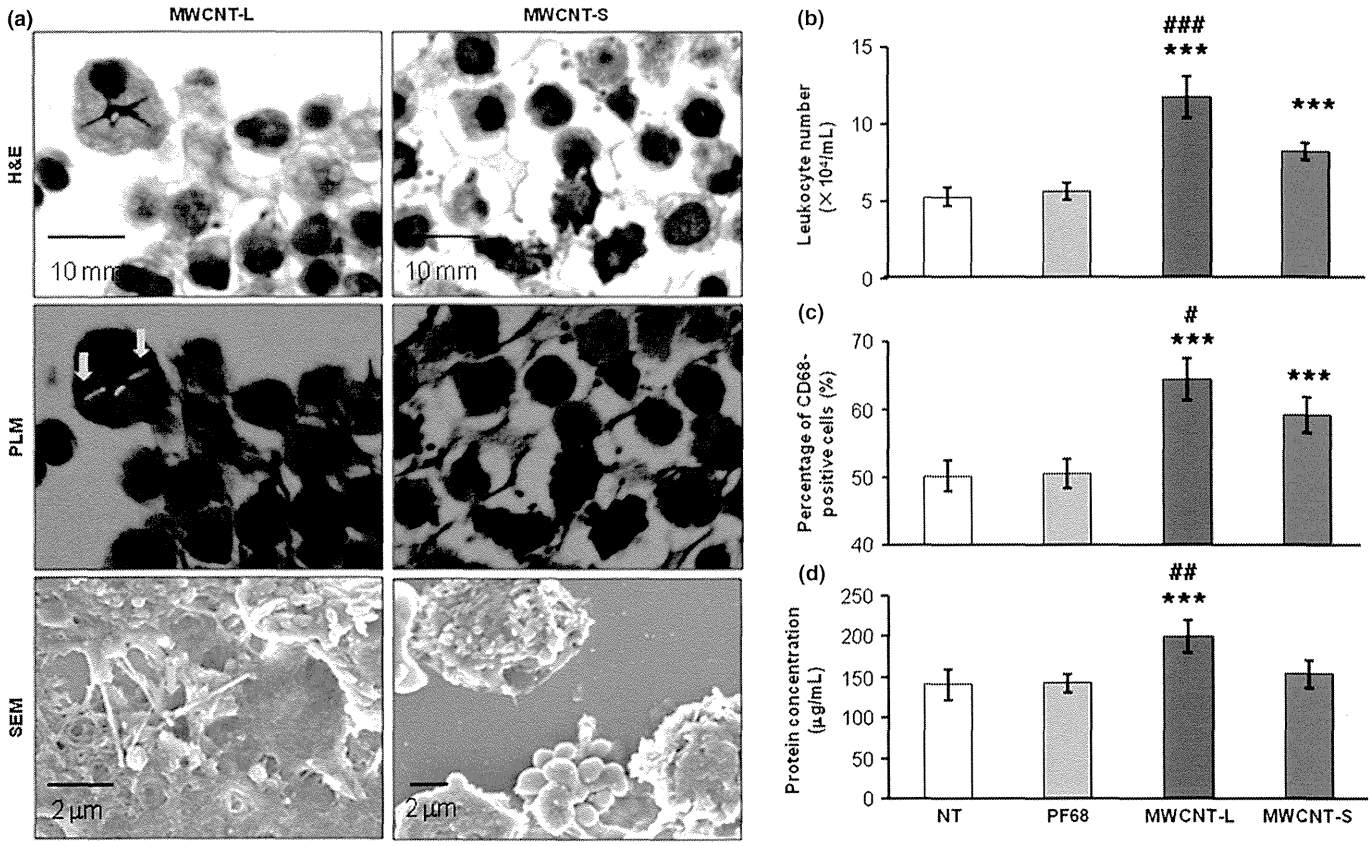

Fig. 4. Demonstration of multiwalled carbon nanotube (MWCNT) fibers and analysis of inflammatory reactions in the pleural cavity. (a) H&E staining, polarized light microscopy (PLM), and SEM images of pleural cell pellets taken from rats treated with larger sized MWCNT (MWCNT-L; l = 8 μm, d = 150 nm) or smaller sized MWCNT (MWCNT-S; l = 3 μm, d = 15 nm). Arrows indicate MWCNT fibers. (b–d) Analysis of leukocyte number (b), proportion of CD 68-positive cells (c), and protein concentration (d) in the supernatants of pleural cavity lavages. ***P < 0.001 versus Pluronic F68 (PF68); #P < 0.05, ##P < 0.01, and ###P < 0.001 MWCNT-L versus MWCNT-S by two-tailed Student's t-test. NT, no treatment.

ble among the PF68, MWCNT-L, and MWCNT-S treated groups (Table 1). Smaller sized MWCNT were more potent than MWCNT-L in inducing 8-hydroxydeoxyguanosine (8-OHdG), a marker for oxidative stress, in the lung tissue (Fig. S3F).

Transportation of MWCNT-L to extrapulmonary organs. In addition to the lung and pleura, MWCNT-L was found in extrapulmonary organs. Polarized light microscopy observations indicated that MWCNT-L was transported to the mediastinal (Fig. S4A), submandibular (Fig. S4B), and mesentery (Fig. S4C) lymph nodes, with many more fibers in the mediastinal lymph nodes than in the other examined lymph nodes. A few MWCNT-L fibers were also observed in the liver (Fig. S4D), kidney (Fig. S4E), spleen (Fig. S4F), and brain (Fig. S4G). Examination with SEM did not detect MWCNT-S in these organs.

Cytotoxicity *in vitro*. Smaller sized MWCNT were more potent than MWCNT-L in lowering cell viability of primary rat alveolar macrophages, human mesothelioma cells, human lung carcinoma cells, and human lung fibroblasts *in vitro* (Fig. S5).

Discussion

Multiwalled carbon nanotubes, when injected into the peritoneal cavity or the scrotum, results in the development of mesothelioma.[11–13] It is of great interest to know whether pulmonary exposure leads to migration of MWCNT into the pleural cavity. Our previous study showed that short-term exposure of the lung to MWCNT resulted in fiber translocation into the pleural cavity and induction of pleural inflammation and fibrosis and mesothelial cell proliferation in the visceral pleura.[15] Similarly, Porter *et al.* and Mercer *et al.* showed that MWCNT could reach the visceral pleura[20] and enter the pleural cavity.[14] Furthermore, Mercer *et al.*[16] showed that MWCNT was transported to the muscle tissue of the chest wall and distant organs. Multiwalled carbon nanotubes were not found in the parietal pleura in these studies, probably due to short exposure periods and/or low doses.

Development of asbestos-induced pleural malignant mesothelioma in humans is a long-term process with a latency of up to tens of years,[2] indicating this is a cumulative effect of the fibers and associated pathogenic responses in the pleura. Thus, accurate modeling of human exposure to asbestos-like fibers and related pathogenesis in rodents is difficult. One solution to this problem is to increase exposure doses in animals. Therefore, in the present study, we sprayed a relatively high dose of MWCNT into the rat lung for a longer exposure period. The dosing was much higher than the recommended exposure limit of 1 μg/m^3 to carbon nanotubes and carbon nanofibers for an 8-h time–weight average proposed by the US National Institute of Occupational Safety and Health in 2013 (http://www.cdc.gov/niosh/docs/2013-145/).

© 2014 The Authors. Cancer Science published by Wiley Publishing Asia Pty Ltd on behalf of Japanese Cancer Association.

Table 1. Cytokines/chemokines in the pleural cavity lavage and lung tissue of rats treated with multiwalled carbon nanotubes (MWCNT)

Cytokines/chemokines	Pleural cavity lavage (pg/mL)			Lung tissue (pg/mg protein)		
	PF68	MWCNT-L	MWCNT-S	PF68	MWCNT-L	MWCNT-S
G-CSF	n.d.	n.d.	n.d.	n.d.	n.d.	n.d.
GM-CSF	n.d.	n.d.	n.d.	n.d.	n.d.	n.d.
MIP1α	n.d.	n.d.	n.d.	63.8 ± 16.2	120.7 ± 21.0***	331.5 ± 90.4***,†††
MIP2	n.d.	n.d.	n.d.	12.4 ± 6.1	27.2 ± 4.9***	59.7 ± 16.7***,††
MCP1	n.d.	n.d.	n.d.	18.0 ± 13.9	39.1 ± 16.3*	213.1 ± 45.8***,†††
TNF-α	n.d.	n.d.	n.d.	n.d.	n.d.	n.d.
IFN-γ	n.d.	n.d.	n.d.	n.d.	n.d.	n.d.
GRO/KC	n.d.	n.d.	n.d.	425.2 ± 194.3	1105.4 ± 395.7**	1353.1 ± 362.6***
IP10	1.5 ± 1.5	8.9 ± 2.3***,†††	2.3 ± 2.3	35.6 ± 5.8	49.9 ± 4.4***	64.0 ± 11.0***,†
RANTES	3.8 ± 0.9	6.9 ± 1.9***,†††	4.1 ± 0.7	556.0 ± 128.6	531.7 ± 127.9††	335.4 ± 61.3**
IL-1α	n.d.	n.d.	n.d.	56.9 ± 14.4	85.3 ± 7.3**	84.5 ± 14.0**
IL-1β	n.d.	n.d.	n.d.	73.0 ± 19.3	103.7 ± 18.6*	154.5 ± 17.6***,†††
IL-4	n.d.	n.d.	n.d.	3.7 ± 3.0	4.2 ± 3.4	3.8 ± 1.9
IL-2	1.2 ± 1.9	14.1 ± 5.5***,††	5.2 ± 5.9	18.3 ± 4.1	18.9 ± 3.0	20.3 ± 7.7
IL-6	n.d.	n.d.	n.d.	29.1 ± 14.1	27.0 ± 13.5	32.6 ± 13.4
IL-12p70	n.d.	n.d.	n.d.	n.d.	n.d.	n.d.
IL-17α	n.d.	n.d.	n.d.	n.d.	n.d.	n.d.
IL-18	66.3 ± 17.0	108.4 ± 25.1**,†	70.4 ± 21.5	2294.8 ± 495.2	2471.8 ± 391.7	3085.6 ± 418.4*,†
VEGF	n.d.	n.d.	n.d.	111.0 ± 24.0	99.1 ± 14.4	201.4 ± 13.8***,†††
EGF	n.d.	n.d.	n.d.	n.d.	n.d.	n.d.

Data are expressed as mean ± standard deviation, $n = 6$ in each treatment group. *$P < 0.05$, **$P < 0.01$, ***$P < 0.001$, larger sized MWCNT (MWCNT-L; $l = 8$ μm, $d = 150$ nm) or smaller sized MWCNT (MWCNT-S; $l = 3$ μm, $d = 15$ nm) versus Pluronic F68 (PF68). †$P < 0.05$, ††$P < 0.01$, †††$P < 0.001$, MWCNT-L versus MWCNT-S. EGF, epidermal growth factor; G-CSF, granulocyte colony-stimulating factor; GM-CSF, granulocyte/macrophage colony-stimulating factor; GRO/KC, growth related oncogene/ keratinocyte-derived cytokine; IFNγ, γ-interferon; IL, interleukin; IP-10, interferon gamma-induced protein 10; n.d., not detectable; TNF-α, tumor necrosis factor-α; MCP1, monocyte chemotactic protein 1; MIP, macrophage inflammatory protein; RANTES, regulated on activation, normal T cell expressed and secreted; VEGF, vascular endothelial growth factor.

The results of this study show that MWCNT-L applied to the lung was found in the pleural cavity and deposited in the parietal pleura, and induced higher inflammatory reactions in the pleural cavity, fibrotic thickening of both the parietal and visceral pleura, and mesothelial proliferation, whereas MWCNT-S caused higher inflammatory reactions and 8-OHdG formation in the lung. Reports have shown that pro-inflammatory cytokines promote mesothelial cell transformation *in vitro*,[21] indicating chronic inflammation is a likely contributing factor in the development of mesothelioma. Due to its length and needle-like shape, MWCNT-L deposited in the pleura, especially in the parietal side, is difficult to clear and results in chronic inflammation in the deposited site. Thus, MWCNT-L has more potential to cause pleural mesothelioma.

It should be noted that properties of MWCNT-L and MWCNT-S, other than size and shape, such as chemical composition (MWCNT-L contains zinc [Fig. S1]) and rigidity,[22] may contribute to the observed different effects in the pleura and lung. Smaller sized MWCNT were not found in the pleural cavity, possibly because MWCNT-S formed cotton candy-like aggregates and very few free fibers translocated from the lung to the pleural cavity, or/and these fibers were rapidly cleared from the pleural cavity. The size- and shape-dependent pleural toxicity shown in our study is consistent with previous reports that direct injection of MWCNT into the pleural cavity leads to length-dependent retention of MWCNT in the pleural cavity and sustained inflammation and fibrosis in the parietal pleura,[17] and with reports that inhaled amosite fibers are found in the parietal pleura with inflammation and fibrosis.[23,24] When we were preparing this manuscript, Murphy *et al.* reported that long MWCNT aspired into the lung of mice was found in the parietal pleura and caused stronger inflammation and fibrosis both in the pleura and lung than short or tangled MWCNT. The lung responses to short or tangled MWCNT are different from our results, possibly due to different animals, administration methods, MWCNT used, and sampling time.[25]

Current administration regulations to set permissible air concentrations of particles and fibers are usually based on lung burdens. Although lung diseases may well be related to the lung burden of specific particles or fibers, lung burden is not always suitable for prediction of pleural toxicity of asbestos-like materials.[2,7] In the present study, MWCNT-S showed higher toxicity in the lung, whereas MWCNT-L was more toxic in the pleural tissue, indicating that the site of deposition and the associated toxicity needs be taken into account in regulating carbon nanotube exposure.

In conclusion, deposition of MWCNT-L and induction of fibrosis and mesothelial cell proliferation in the parietal pleura indicate that larger sized MWCNT has greater potential to induce asbestos-like pleural lesions.

Acknowledgments

This work was supported by Health and Labor Sciences Research Grants of Japan (Research on Risk of Chemical Substance 21340601, grant nos. H22-kagaku-ippan-005, H24-kagaku-sitei-009, and H25-kagaku-ippan-004) and by the Princess Takamatsu Cancer Research Fund (H24).

Disclosure Statement

The authors have no conflict of interests.

© 2014 The Authors. Cancer Science published by Wiley Publishing Asia Pty Ltd on behalf of Japanese Cancer Association.

References

1 Boutin C, Rey F, Gouvernet J, Viallat JR, Astoul P, Ledoray V. Thoracoscopy in pleural malignant mesothelioma: a prospective study of 188 consecutive patients. Part 2: prognosis and staging. *Cancer* 1993; **72**: 394–404.
2 Cugell DW, Kamp DW. Asbestos and the pleura: a review. *Chest* 2004; **125**: 1103–17.
3 Kane AB. Mechanisms of mineral fibre carcinogenesis. *IARC Sci Publ* 1996; **140**: 11–34.
4 Robinson BW, Musk AW, Lake RA. Malignant mesothelioma. *Lancet* 2005; **366**: 397–408.
5 Boutin C, Dumortier P, Rey F, Viallat JR, De Vuyst P. Black spots concentrate oncogenic asbestos fibers in the parietal pleura. Thoracoscopic and mineralogic study. *Am J Respir Crit Care Med* 1996; **153**: 444–9.
6 Kohyama N, Suzuki Y. Analysis of asbestos fibers in lung parenchyma, pleural plaques, and mesothelioma tissues of North American insulation workers. *Ann N Y Acad Sci* 1991; **643**: 27–52.
7 Donaldson K, Murphy FA, Duffin R, Poland CA. Asbestos, carbon nanotubes and the pleural mesothelium: a review of the hypothesis regarding the role of long fibre retention in the parietal pleura, inflammation and mesothelioma. *Part Fibre Toxicol* 2010; **7**: 5.
8 Bonner JC. Nanoparticles as a potential cause of pleural and interstitial lung disease. *Proc Am Thorac Soc* 2010; **7**: 138–41.
9 Nagai H, Toyokuni S. Biopersistent fiber-induced inflammation and carcinogenesis: lessons learned from asbestos toward safety of fibrous nanomaterials. *Arch Biochem Biophys* 2010; **502**(1): 1–7.
10 Poland CA, Duffin R, Kinloch I *et al.* Carbon nanotubes introduced into the abdominal cavity of mice show asbestos-like pathogenicity in a pilot study. *Nat Nanotechnol* 2008; **3**: 423–8.
11 Sakamoto Y, Nakae D, Fukumori N *et al.* Induction of mesothelioma by a single intrascrotal administration of multi-wall carbon nanotube in intact male Fischer 344 rats. *J Toxicol Sci* 2009; **34**(1): 65–76.
12 Takagi A, Hirose A, Futakuchi M, Tsuda H, Kanno J. Dose-dependent mesothelioma induction by intraperitoneal administration of multi-wall carbon nanotubes in p53 heterozygous mice. *Cancer Sci* 2012; **103**: 1440–4.
13 Takagi A, Hirose A, Nishimura T *et al.* Induction of mesothelioma in p53+/− mouse by intraperitoneal application of multi-wall carbon nanotube. *J Toxicol Sci* 2008; **33**: 105–16.
14 Mercer RR, Hubbs AF, Scabilloni JF *et al.* Distribution and persistence of pleural penetrations by multi-walled carbon nanotubes. *Part Fibre Toxicol* 2010; **7**: 28.
15 Xu J, Futakuchi M, Shimizu H *et al.* Multi-walled carbon nanotubes translocate into the pleural cavity and induce visceral mesothelial proliferation in rats. *Cancer Sci* 2012; **103**: 2045–50.
16 Mercer RR, Scabilloni JF, Hubbs AF *et al.* Extrapulmonary transport of MWCNT following inhalation exposure. *Part Fibre Toxicol* 2013; **10**(1): 38.
17 Murphy FA, Poland CA, Duffin R *et al.* Length-dependent retention of carbon nanotubes in the pleural space of mice initiates sustained inflammation and progressive fibrosis on the parietal pleura. *Am J Pathol* 2011; **178**: 2587–600.
18 Schinwald A, Murphy FA, Prina-Mello A *et al.* The threshold length for fiber-induced acute pleural inflammation: shedding light on the early events in asbestos-induced mesothelioma. *Toxicol Sci* 2012; **128**: 461–70.
19 Xu J, Futakuchi M, Iigo M *et al.* Involvement of macrophage inflammatory protein 1alpha (MIP1alpha) in promotion of rat lung and mammary carcinogenic activity of nanoscale titanium dioxide particles administered by intrapulmonary spraying. *Carcinogenesis* 2010; **31**: 927–35.
20 Porter DW, Hubbs AF, Mercer RR *et al.* Mouse pulmonary dose- and time course-responses induced by exposure to multi-walled carbon nanotubes. *Toxicology* 2010; **269**: 136–47.
21 Wang ZL. Functional oxide nanobelts: materials, properties and potential applications in nanosystems and biotechnology. *Annu Rev Phys Chem* 2004; **55**: 159–96.
22 Nagai H, Okazaki Y, Chew SH *et al.* Diameter and rigidity of multiwalled carbon nanotubes are critical factors in mesothelial injury and carcinogenesis. *Proc Natl Acad Sci U S A* 2011; **108**: E1330–8.
23 Bernstein DM, Rogers RA, Sepulveda R *et al.* The pathological response and fate in the lung and pleura of chrysotile in combination with fine particles compared to amosite asbestos following short-term inhalation exposure: interim results. *Inhal Toxicol* 2010; **22**: 937–62.
24 Bernstein DM, Rogers RA, Sepulveda R *et al.* Quantification of the pathological response and fate in the lung and pleura of chrysotile in combination with fine particles compared to amosite-asbestos following short-term inhalation exposure. *Inhal Toxicol* 2011; **23**: 372–91.
25 Murphy FA, Poland CA, Duffin R, Donaldson K. Length-dependent pleural inflammation and parietal pleural responses after deposition of carbon nanotubes in the pulmonary airspaces of mice. *Nanotoxicology* 2013; **7**: 1157–67.

Supporting Information

Additional supporting information may be found in the online version of this article:

Fig. S1. Characterization of multiwalled carbon nanotubes.

Fig. S2. Determination of the thickness of the pleura in rats treated with multiwalled carbon nanotubes.

Fig. S3. Granuloma formation, alveolar macrophage infiltration, and 8-hydroxydeoxyguanosine (8-OHdG) induction in the lung.

Fig. S4. Transportation of larger sized multiwalled carbon nanotubes to extrapulmonary organs.

Fig. S5. Cytotoxicity of multiwalled carbon nanotubes *in vitro*.

© 2014 The Authors. Cancer Science published by Wiley Publishing Asia Pty Ltd on behalf of Japanese Cancer Association.

Arch Toxicol (2014) 88:65–75
DOI 10.1007/s00204-013-1086-5

INORGANIC COMPOUNDS

Nanosized zinc oxide particles do not promote DHPN-induced lung carcinogenesis but cause reversible epithelial hyperplasia of terminal bronchioles

Jiegou Xu · Mitsuru Futakuchi · David B. Alexander · Katsumi Fukamachi · Takamasa Numano · Masumi Suzui · Hideo Shimizu · Toyonori Omori · Jun Kanno · Akihiko Hirose · Hiroyuki Tsuda

Received: 25 February 2013 / Accepted: 20 June 2013 / Published online: 6 July 2013
© The Author(s) 2013. This article is published with open access at Springerlink.com

Abstract Zinc oxide (ZnO) is known to induce lung toxicity, including terminal bronchiolar epithelial hyperplasia, which gives rise to concerns that nanosized ZnO (nZnO) might lead to lung carcinogenesis. We studied the tumor promoting activity of nZnO by an initiation–promotion protocol using human c-Ha-*ras* proto-oncogene transgenic rats (H*ras*128 rats). The rats were given 0.2 % N-nitrosobis(2-hydroxypropyl)amine (DHPN) in the drinking water for 2 weeks and then treated with 0.5 ml of 250 or 500 μg/ml nZnO suspension by intra-pulmonary spraying once every 2 weeks for a total of 7 times. Treatment with nZnO particles did not promote DHPN-induced lung carcinogenesis. However, nZnO dose-dependently caused epithelial hyperplasia of terminal bronchioles (EHTB) and fibrosis-associated interstitial pneumonitis (FAIP) that were independent of DHPN treatment. Tracing the fate of EHTB lesions in wild-type rats indicated that the hyperplastic lesions almost completely disappeared within 12 weeks after the last nZnO treatment. Since nZnO particles were not found in the lung and $ZnCl_2$ solution induced similar lung lesions and gene expression profiles, the observed lesions were most likely caused by dissolved Zn^{2+}. In summary, nZnO did not promote carcinogenesis in the lung and induced EHTB and FAIP lesions that regressed rapidly, probably due to clearance of surplus Zn^{2+} from the lung.

Keywords Nanosized zinc oxide particles · Lung toxicity · Lung carcinogenesis · Epithelial hyperplasia of terminal bronchioles · Interstitial pneumonitis · Lung fibrosis

Electronic supplementary material The online version of this article (doi:10.1007/s00204-013-1086-5) contains supplementary material, which is available to authorized users.

J. Xu · D. B. Alexander · H. Tsuda (✉)
Laboratory of Nanotoxicology Project, Nagoya City University, 3-1 Tanabedohri Mizuho-ku, Nagoya 467-8603, Japan
e-mail: htsuda@phar.nagoya-cu.ac.jp

J. Xu · M. Futakuchi · K. Fukamachi · T. Numano · M. Suzui
Department of Molecular Toxicology, Nagoya City University Graduate School of Medical Sciences, 1-Kawasumi, Mizuho-cho, Mizuho-ku, Nagoya 467-8601, Japan

H. Shimizu
Core Laboratory, Nagoya City University Graduate School of Medical Sciences, 1-Kawasumi, Mizuho-cho, Mizuho-ku, Nagoya 467-8601, Japan

T. Omori
Department of Health Care Policy and Management, Nagoya City University Graduate School of Medical Sciences, 1-Kawasumi, Mizuho-cho, Mizuho-ku, Nagoya 467-8601, Japan

J. Kanno · A. Hirose
National Institute of Health Sciences, 1-18-1 Kamiyoga, Setagaya-ku, Tokyo 158-8501, Japan

Introduction

One of the most widely used nanomaterials is nZnO. The worldwide production of nZnO powder is increasing every year and was reported to have reached 1.4 million tons in 2011. It is used in rubber industry and electronics and in commercial products such as sunscreens and paints. In the biomedical field, it is used in baby powders, antiseptic ointments, and zinc oxide tapes to treat a variety of skin conditions (Baldwin et al. 2001; Hughes and McLean 1988). Recently, nZnO has gained interest in cancer applications or as an active anticancer drug (Rasmussen et al. 2010).

Micron or larger-sized ZnO particles are considered to be "Generally Recognized as Safe" (GRAS) in food

additives by the FDA. However, exposure to fumes containing ZnO and other metal particles during welding or galvanizing processes is known to lead to metal fume fever (Antonini et al. 2003; Drinker and Fairhall 1933; Fine et al. 1997). Recent reports have shown that nZnO affects cell viability and induces reactive oxygen species (ROS) in many mammary cell types in tissue culture (Deng et al. 2009; Lee et al. 2008; Xia et al. 2008; Yang et al. 2009), cause proliferation of airway epithelial cells, goblet cell hyperplasia, interstitial pulmonary inflammation and fibrosis (Cho et al. 2011), and reversible inflammatory reaction in the bronchoalveolar lavage fluid in animal studies (Sayes et al. 2007; Warheit et al. 2009). nZnO also leads to DNA damage (Kermanizadeh et al. 2012) and micronuclei formation in vitro (Valdiglesias et al. 2013). While these in vitro and in vivo studies have provided some information on acute toxic effects of nZnO on certain cell types and animals, further in vivo studies are needed to determine whether nZnO has chronic toxic effects as in some other metal oxide particles. For example, epidemiological data indicate that exposures of aluminum oxide or iron oxide lead to pneumoconiosis in human (Hull and Abraham 2002; Sano 1963); titanium dioxide has carcinogenic activity in the rat lung (Heinrich et al. 1995; Xu et al. 2010). Such chronic toxicity data will have more impact on risk assessment of nZnO.

Since nZnO induces inflammatory reaction, ROS production, and genotoxicity, which are implicated in cancer development, in the present study, we tested the lung carcinogenicity of nZnO by an initiation–promotion protocol using human c-Ha-*ras* proto-oncogene transgenic (H*ras* 128) rats, which have the same susceptibility to chemically induced lung carcinogenesis as their parent wild-type rats, but are highly susceptible to mammary tumor induction (Tsuda et al. 2005). The results indicated that nZnO did not have promotion effect on DHPN-induced lung and mammary carcinogenesis and caused reversible EHTB and FAIP.

Materials and methods

Animals

Forty-three female transgenic rats carrying the human c-Ha-RAS proto-oncogene (H*ras*128 rats) and 42 female wild-type Sprague–Dawley rats were obtained from CLEA Japan Co., Ltd. (Tokyo, Japan). The animals were housed in the Animal Center of Nagoya City University Medical School and maintained on a 12-h light/12-h dark cycle and received Oriental MF basal diet (Oriental Yeast Co. Ltd., Tokyo, Japan) and water ad libitum. The study was conducted according to the Guidelines for the Care and Use of Laboratory Animals of Nagoya City University Medical School, and the experimental protocol was approved by the Institutional Animal Care and Use Committee (H22M-19).

Preparation, characterization of nZnO suspensions, and administration of nZnO to the lung

Zinc oxide particles (CAS No. 1314-13-2, MZ-500, without coating, with a mean primary diameter of 25 nm) were obtained from Tayca Cooperation, Osaka, Japan. The particles were suspended in 0.1 % Tween 20 saline at 250 or 500 μg/ml. The suspension was sonicated for 20 min to prevent aggregate formation.

Characterization of nZnO was conducted as follows: the shape of nZnO in the suspensions was imaged by transmission electron microscopy (TEM); element analysis was performed by an X-ray microanalyzer (EDAX, Tokyo, Japan), after aliquots of nZnO were loaded on a carbon sheet; the size distribution of nZnO in the 500 μg/ml suspension was analyzed using a Particle Size Distribution Analyzer (Shimadzu Techno-Research, Inc., Kyoto, Japan). The characterization results are shown in Figure S1.

Before being administrated to rats, the nZnO suspensions were further sonicated for 20 min. 0.5 ml of the nZnO suspensions was administrated to the lung by intra-pulmonary spraying (IPS) as described previously (Xu et al. 2010).

Carcinogenicity study

The carcinogenic activity of nZnO was assessed in female H*ras*128 rats using an initiation–promotion protocol by which we used previously to evaluate lung and mammary carcinogenicity of titanium dioxide nanoparticles (Xu et al. 2010). Briefly, three groups of 10–11 female H*ras*128 rats aged 6 weeks were given 0.2 % DHPN (Wako Chemicals, Co., Ltd. Osaka, Japan) in the drinking water for 2 weeks, and Groups 4 and 5 (6 rats each) were given drinking water without DHPN. Two weeks later, Group 1 and Group 4 were administered 0.1 % Tween 20 saline, and Group 2, Group 3, and Group 5 were administered 250, 500, and 500 μg/ml nZnO suspensions by IPS once every two weeks from the end of week 4 to week 16, a total of 7 times. The total amounts of nZnO administered to Groups 1, 2, 3, 4, and 5 were 0, 0.875, 1.75, 0, and 1.75 mg/rat, respectively. The dosing was determined according to the permissible exposure limit for zinc oxide particles of the Occupational Safety and Health Administration (OSHA) (see Discussion). Three days after the last treatment, animals were killed and the organs (brain, lung, liver, spleen, kidney, mammary gland, ovaries, uterus, and neck lymph nodes) were fixed in 4 % paraformaldehyde in PBS buffer adjusted to pH 7.3 and processed for histological examination and transmission electron microscopy (TEM).

Light microscopy, polarized light microscopy, and transmission electron microscopy

Hematoxylin–Eosin (H&E)-stained pathological slides of the lung and other major organs were used to observe nZnO with a light microscope and polarized light microscope (PLM) (Olympus BX51N-31P-O polarized light microscope, Tokyo, Japan) at 1,000× magnification. Localization of the illuminated particles was confirmed in the same H&E-stained sections after removing the polarizing filter.

Paraffin blocks were deparaffinized and embedded in epon resin and processed for nZnO observation and zinc element analysis, using a JEM-1010 transmission electron microscope (TEM) (JEOL, Co. Ltd, Tokyo, Japan) equipped with an X-ray microanalyzer (EDAX, Tokyo, Japan).

Immunohistochemistry and Azan–Mallory staining

PCNA was detected using an anti-PCNA monoclonal antibody (Clone PC10, Dako Japan Inc., Tokyo, Japan). The antibody was diluted 1:200 in blocking solution and applied to deparaffinized slides, and the slides were incubated at 4 °C overnight. The slides were then incubated for 1 h with biotinylated species-specific secondary antibodies diluted 1:500 (Vector Laboratories, Burlingame, CA) and visualized using avidin-conjugated horseradish peroxidase complex (ABC kit, Vector Laboratories). To assess lung fibrosis, paraffin-embedded slides were deparaffinized, and collagen fibers were visualized by Azan–Mallory staining.

Reversibility study and effects of $ZnCl_2$ solution

To assess whether nZnO-induced terminal bronchiolar epithelial hyperplasia, interstitial pneumonitis, and lung fibrosis are reversible, we conducted reversibility experiments. Seven groups of 5 female wild-type Sprague–Dawley rats aged 10 weeks were administrated 0.5 ml of 0.1 % Tween 20 saline or 500 μg/ml nZnO suspension by IPS 2 times per week for 4 weeks. Group 1 was treated with 0.1 % Tween 20 saline and killed 1 day after the last IPS. Groups 2–7 were treated with 0.5 ml of 500 μg/ml nZnO suspension and killed at 1 day and 2, 4, 6, 8, and 12 weeks after the last IPS. For the comparison of the effects of zinc ion and nZnO, Group 8 was treated with 0.5 ml of 6.17 mM $ZnCl_2$ solution (the molecular amount is equal to that of 500 μg/ml nZnO suspension) by IPS at the same frequency and time period as the nZnO groups and killed 1 day after the last IPS. The left lung was cut into pieces and frozen in liquid nitrogen for biochemical analysis, and the right lung was processed for histological examination. Other major organs were excised for histological examination, and the blood was collected for cytological and biochemical analysis.

Gene expression analysis

The left lungs from Groups 1, 2, and 8 in the reversibility study described above were used for isolation of RNA. RNA was isolated by using TRizol reagent (Invitrogen of Life Technologies, CA).

For microarray analysis, 1 μg RNA from each rat of Group 1 was combined and 1 μg RNA from each rat of Group 2 was combined. The quality of the 2 mixtures of RNA samples was assessed and quantified using the Agilent 2100 BioAnalyzer RNA Nano chip system (Agilent Technologies, CA) prior to further manipulation. Microarray analysis was conducted by the 3-D Gene Chip (Toray Industries Inc., Kanagawa, Japan), and a total of 20,000 genes were analyzed. Microarray-based pathway analysis was performed by Toray Industries Inc., Kanagawa, Japan.

For reverse transcription-PCR (RT-PCR) and real-time PCR, first-strand cDNA synthesis from 1 μg of RNA was performed using SuperScript™ III First-Strand Synthesis System (Invitrogen of Life Technologies, CA) according to the manufacturer's instructions. Primers are as follows: forward primer, 5′-TAGAATCGAGGTGCACAGGAGT-3′, reverse primer, 5′-TATTCCAGCAGGCTGTCAAAGA-3′, product size, 228 bp for Orm1; forward primer, 5′-AAGTGGAGGAGCAGCTGGAGTGG-3′, reverse primer, 5′-CCAAAGTAGACCTGCCCGGACTC-3′, product size, 155 bp for Tnfa, and forward primer, 5′-AGCCATGTACGTAGCCATCC-3′, reverse primer, 5′-CTCTCAGCTGTGGTGGTGAA-3′, product size, 228 bp for Actb. RT-PCR was conducted using an iCycler (BioRad Life Sciences, CA) as follows: 95 °C 20 s, 60 °C 20 s, 72 °C 30 s, 30 cycles for Orm1; 95 °C 20 s, 60 °C 20 s, 72 °C 20 s, 25 cycles for Tnfa, and 95 °C 20 s, 60 °C 20 s, 72 °C 30 s, 15 cycles for Actb. Real-time PCR analysis of Orm1 and Tnfa gene expression was performed with the 7300 real-time PCR system (Applied Biosystem, CA) using the premix reagent Power SYBR Green PCR Master Mix (Applied Biosystem, CA) according to the manufacturer's instructions. The Actb gene was used as the normalizing reference gene.

Determination of zinc ion

For detection of Zn^{2+} content in the lung tissue, 50–100 mg of the frozen lung tissues from the reversibility study described above were thawed at room temperature, rinsed with cold PBS 3 times, and homogenized for 30 s at the highest speed in 1 ml of T-PER, tissue protein extraction reagent (Pierce, Rockford, IL), with Polytron R PT 2100 homogenizer (Capitol Scientific Inc., TX). The homogenates were clarified by centrifugation at 10,000×g for 15 min at 4 °C, and the supernatants were used for Zn^{2+}

detection. Zn^{2+} detection was performed using QuantiChrom™ Zinc Assay kit (BioAssay Systems, CA) according to the manufacturer's instructions.

In vitro nZnO dissolution assay

5 μl of 500 μg/ml nZnO suspension (2.5 μg/tube) and increasing amounts of 1 mg/ml human α 1 acid glycoprotein (Sigma-Aldrich, product number G9885) or bovine serum albumin (Sigma-Aldrich, product number A2058) were added to microtubes, and the total volume of each tube was adjusted to 100 μl with 0.1 % Tween 20 saline. The final protein concentration of human α 1 acid glycoprotein or bovine serum albumin was 0, 100, 200, 300, 400, and 500 μg/ml. The tubes were then incubated at 37 °C for 2 h. The nZnO particles were removed by centrifugation at 10,000×*g* for 5 min, and Zn^{2+} concentration in the supernatants was determined as described above.

In vitro cytotoxicity assay

The induction and preparation of rat primary alveolar macrophages (PAM) has been described (Xu et al. 2010). 5×10^3 PAMs, 1×10^3 A549 cells (human lung adenocarcinoma cell line), and 2×10^3 CCD34 cells (human lung fibroblast cell line) were seeded into 96-well culture plates and cultured overnight in 100 ml of RPMI 1,640 containing 10 % FBS. The cells were added with nZnO suspension or ZnCl2 solution to final concentrations of 0, 1, 5, or 25 μg/ml of nZnO and 0, 12.3, 61.7, or 308.6 nM of ZnCl2 (1, 5, and 25 μg/ml of nZnO are equal to 12.3, 61.7, and 308.6 nM of ZnCl2, respectively, in the amount of zinc element) and incubated for another 72 h. The cell viability was then determined using the Cell Counting Kit-8 (Dojindo Molecular Technologies, Rockville, MD) according to the manufacturer's instruction.

Statistical analysis

Statistical analysis was performed using ANOVA. Statistical significance was analyzed using a two-tailed Student's *t*-test. A p value of <0.05 was considered to be significant.

Results

Carcinogenesis study in H*ras*128 rats

DHPN-induced lung alveolar cell hyperplasia and adenoma development was used for the end point observation to assess the carcinogenicity of nZnO in our medium-term assay. As shown in Table 1, the incidence and multiplicity (number/cm^2 lung tissue section) of

Table 1 Effect of nZnO on lung proliferative lesions in H128-*ras* rats

Treatment	No. of rats	DHPN-induced proliferative lesions						DHPN-independent EHTB[a]	
		ACH[a]		Ade[a]		ACH + Ade		Inc. (%)	Multiplicity[b] (no./cm^2 lung)
		Inc.[a] (%)	Multiplicity[b] (no./cm^2 lung)	Inc. (%)	Multiplicity[b] (no./cm^2 lung)	Inc. (%)	Multiplicity[b] (no./cm^2 lung)		
DHPN + vehicle	11	11 (100)	2.43 ± 1.29	2 (18.1)	0.09 ± 0.20	11 (100)	2.52 ± 1.26	0 (0)	0
DHPN + 250 μg/ml nZnO	10	10 (100)	1.64 ± 1.09	3 (30.0)	0.12 ± 0.19	10 (100)	1.76 ± 1.03	7 (70)	0.86 ± 0.86 **
DHPN + 500 μg/ml nZnO	10	10 (100)	1.83 ± 1.05	5 (50.0)	0.30 ± 0.31	10 (100)	2.13 ± 1.23	10 (100)	4.93 ± 1.95 ***
Vehicle	6	0	0	0	0	0	0	0	0
500 μg/ml nZnO	6	2 (33.3)	0.16 ± 0.26	0	0	2 (33.3)	0.16 ± 0.26	6 (100)	3.91 ± 1.29 ***

[a] ACH, Ade, EHTB, and Inc. are abbreviations for alveolar cell hyperplasia, adenoma, epithelial hyperplasia of terminal bronchioles, and incidence, respectively

[b] Multiplicity is expressed as mean ± s.d

** and *** represent p values <0.01 and 0.001, respectively, versus DHPN + vehicle or vehicle

alveolar cell hyperplasia and adenoma in the groups treated with nZnO were not significantly different from the DHPN alone group. In the rats which received nZnO treatment without prior DHPN treatment, alveolar cell proliferation foci, recognized as thickening of the alveolar wall with proliferative alveolar epithelium, were observed, but significant differences from the saline group were not observed. In the mammary gland, significant inter-group difference in incidence and multiplicity of mammary tumors was also not observed (data not shown).

A notable lesion induced in all the nZnO-treated groups was epithelial hyperplasia of terminal bronchioles (EHTB). The EHTB lesions had increased cell density, often with the epithelial cells arranged in 1–3 layers, and partly extended bronchiolar structures with transition to the normal

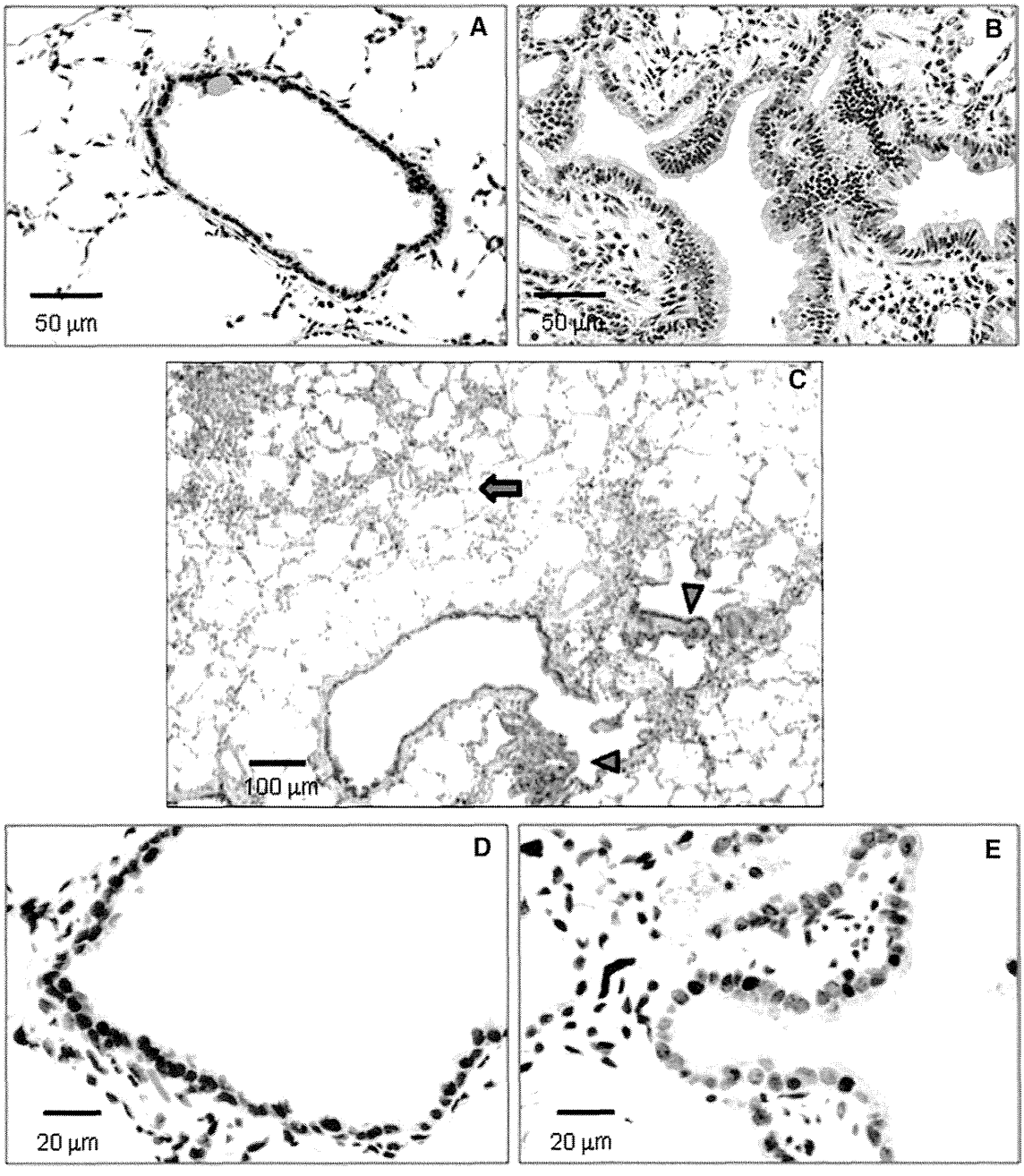

Fig. 1 Induction of EHTB by nZnO. **a** representative normal terminal bronchiolar epithelium (NTBE); **b** EHTB in H&E-stained slides; **c** images and localizations of DHPN-induced alveolar hyperplasia (*arrow*) and nZnO-induced EHTB (*arrow heads*); **d** images of PCNA immunostaining in NTBE; and **e** in EHTB

terminal bronchioles (Fig. 1a, b). The EHTB lesions were independently localized from the DHPN-induced alveolar cell hyperplastic lesions (Fig. 1c). The incidences and multiplicity (number/cm^2 lung tissue section) of EHTB in the groups treated with nZnO were significantly increased compared with that of the DHPN alone group. The increase was dose-dependent (Spearman rank correlation test, $p < 0.001$) (Table 1). Immunostaining with proliferating cell nuclear antigen (PCNA) indicated that proliferating bronchiolar epithelial cells were preferentially found in the EHTB lesions, but rarely found in the normal terminal bronchial epithelial areas (Fig. 1d, e).

Another lesion found in the groups treated with nZnO, and also independent of DHPN treatment, was interstitial pneumonitis (Fig. 2a). The lesion was usually associated with fibrosis of various thicknesses of the septal wall extruding into the alveolar structure (blue staining in Fig. 2b). Quantitative analysis indicated a significant increase in the fibrotic area in the rats treated with nZnO compared with that of rats treated with DHPN alone (Fig. 2c), and the increase was dose-dependent (Spearman rank correlation test, $p < 0.001$). In addition, the EHTB lesions often occurred near or within interstitial pneumonitis areas.

Light microscopic observation of the alveoli of the rats treated with nZnO showed infiltration of numerous macrophages mixed with a few neutrophils, eosinophils, and lymphocytes (data not shown). The nZnO particles were not found in any of the alveolar macrophages; these macrophages contained numerous vacuolar vesicles in the cytoplasm (Fig. 2d). Transmission electron microscopic (TEM) observation showed that nZnO particles were not found within the vacuolar vesicles (Fig. 2e) or in any alveolar tissue cells (Fig. 2f). The absence of a zinc peak was confirmed by elemental scanning with TEM-X-ray microanalysis (Figure S2). nZnO particles were also not detected under polarized light microscope observation. This feature was in contrast with titanium dioxide nanoparticles which were clearly observed in alveolar macrophages (Figure S3).

Reversibility of EHTB and FAIP in wild-type rats

As in the H*ras*128 transgenic rats, nZnO induced EHTB and FAIP in wild-type Sprague–Dawley (SD) rats (Fig. 3a), and nZnO was not found in the lung tissue. nZnO-induced EHTB and FAIP gradually regressed with time (Fig. 3a), and the number of EHTB foci per square centimeter lung tissue section decreased from 9.81 ± 1.42 at day 1 to 0.06 ± 0.13 at week 12 after cessation of nZnO exposure (Fig. 3b). The total Zn^{2+} content in the lung tissue also gradually decreased (Fig. 3c) and was positively correlated with the number of EHTB ($r = 0.96$ by Pearson correlation test).

Microarray analysis

Microarray analysis of the lung tissue indicated that nZnO treatment up-regulated the expression of 738 genes and down-regulated the expression of 267 genes (data not shown). The up-regulated inflammation-associated genes included chemotactic chemokines such as Cxcl5, Cxcl11, Ccl7, Cxcl2, Ccl2, and Cxcl1, proinflammatory cytokines such as Tnfa and Il6, and the acute-phase reactant Orm1 (Table S1). Pathway analysis showed an increase in inflammatory responses in which macrophages and TNFα play a central role (Figure S4). The gene expression profiling was consistent with the strong inflammatory responses in the lung observed by histological examination. Other pathways up-regulated by nZnO included classical complement activation pathway, matrix metalloproteinase pathway, cholesterol biosynthesis pathway and striated muscle contraction pathway, and treatment of nZnO down-regulated the adipogenesis pathway (data not shown).

Effects of $ZnCl_2$ solution on the lung of wild-type rats

To check whether the nZnO-induced EHTB and FAIP were due to dissolution of nZnO to Zn^{2+}, we administered $ZnCl_2$ solution (the molecular amount is equal to that of 500 μg/ml nZnO suspension) to the lung of rats by IPS. The lesions were histologically similar to those observed in the nZnO-treated rats (Fig. 4a, b, c). Quantitative analysis of EHTB indicated that the number of EHTB induced by $ZnCl_2$ solution and nZnO was comparable (Fig. 4d).

To examine whether Zn^{2+} and nZnO have the same underlying molecular mechanisms, two genes, Tnfa and Orm1, which were determined to be up-regulated in the nZnO-treated rats by microarray analysis, were chosen for gene expression analysis. These genes were chosen because Tnfa-encoded tumor necrosis factor alpha is a multifunctional proinflammatory cytokine involved in a variety of acute and chronic inflammatory responses, and Orm1-encoded alpha 1 acid glycoprotein (AGP) is an acute-phase protein usually synthesized by hepatocytes in response to trauma, infection, and inflammation (Fournier et al. 2000). RT-PCR (Fig. 4e) and real-time PCR (Fig. 4f) showed that treatment with both $ZnCl_2$ solution and nZnO increased the expression of Tnfa and Orm1 genes in the lung tissue, with a little higher induction in the $ZnCl_2$ solution treated rats. Similarly, increased expression of Orm1 genes was found in primary alveolar macrophages exposed to nZnO in vitro (Fig. 4g). Interestingly, addition of human AGP to nZnO suspension dose-dependently promoted dissolution of nZnO from 59.1 nmol/ml (19.7 % dissolved,

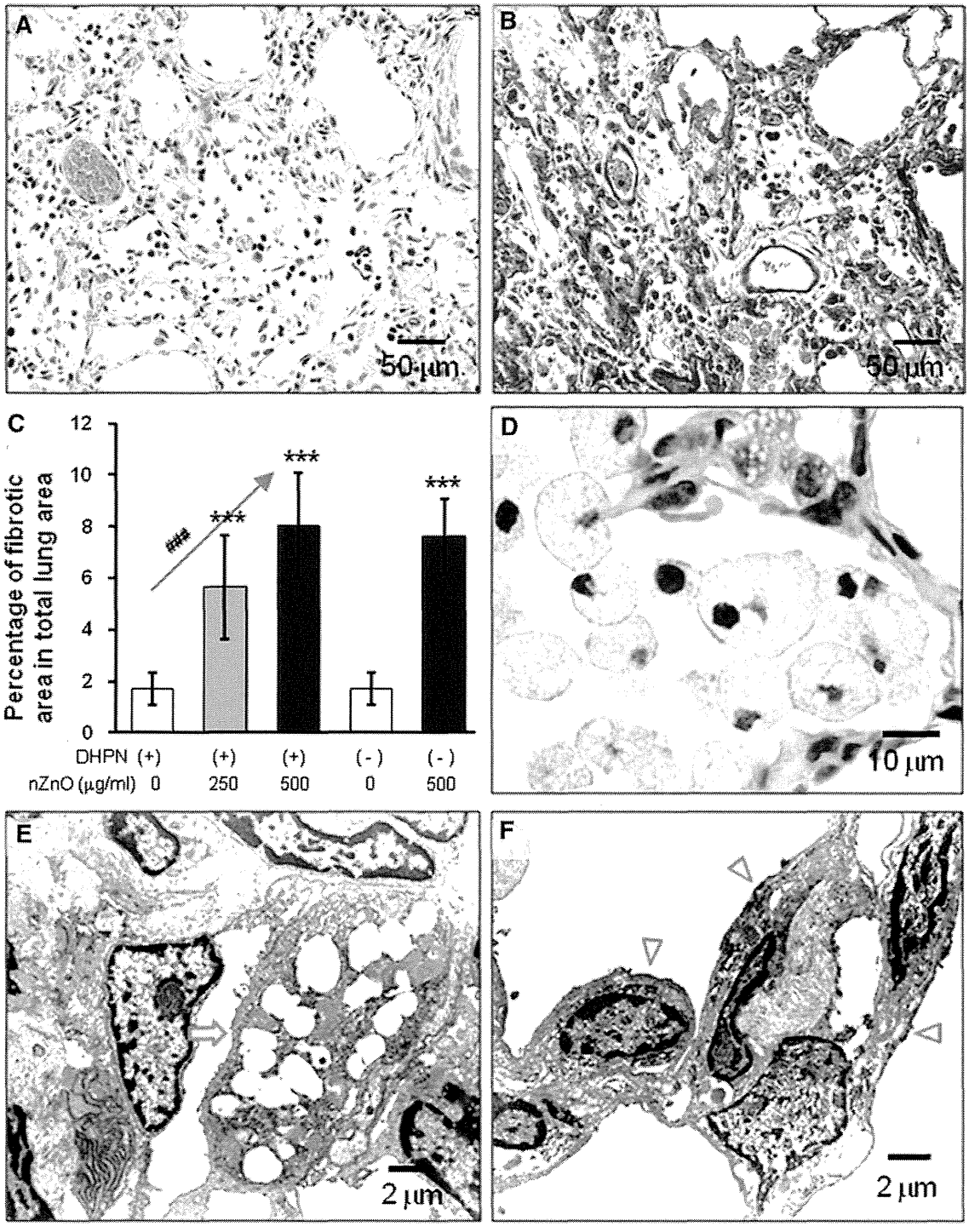

Fig. 2 Induction of FAIP and observation of nZnO particles. **a** representative image of FAIP in rats treated with nZnO; **b** image of Azan–Mallory staining in the lung of rats treated with nZnO, showing collagen fibers; **c** percentage of the fibrotic area in total lung tissue area. ***<0.001 by two-tailed Student's *t*-test versus the vehicle group; and ###$p < 0.001$ by Spearman rank correlation test. **d** image showing alveolar macrophages with vacuous phagocytosis vesicles; **e** and **f** TEM images showing alveolar macrophages (*arrow*) and epithelium (*arrow heads*), no nZnO particles being observed

without addition of AGP) to 117.3 nmol/ml (39.1 % dissolved after addition of 500 μg/ml of AGP), while addition of bovine serum albumin (BSA) had little effect on dissolution of nZnO (Fig. 4h). Exposure of both nZnO and $ZnCl_2$ solution resulted in dose-dependent cell death in vitro (Figure S5).

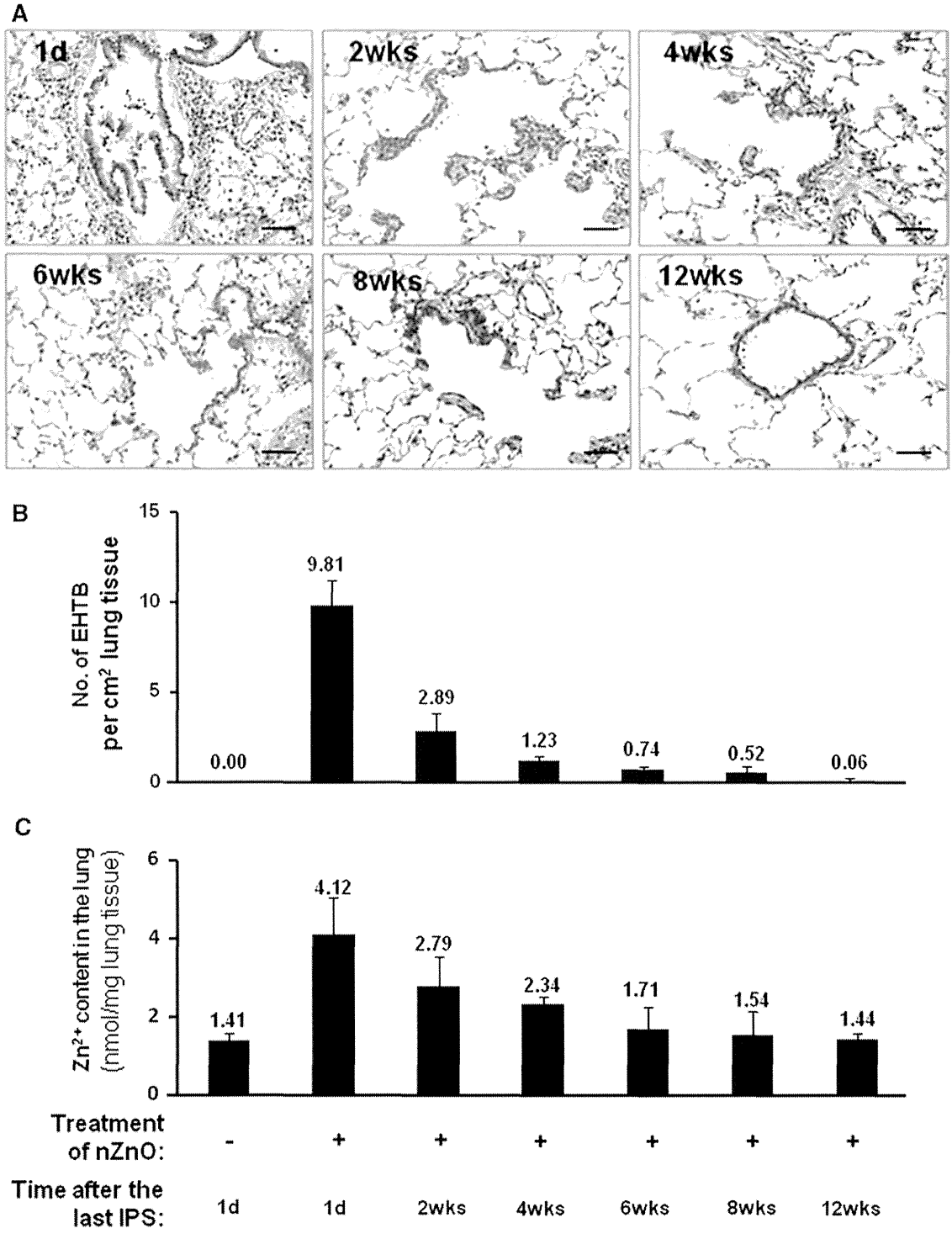

Fig. 3 nZnO-induced EHTB and FAIP are reversible. Wild-type rats were treated with 500 μg/ml nZnO by IPS 2 times/week for 4 weeks and killed at different time points of 1 day (1d) and 2, 4, 6, 8, and 12 weeks (wks) after the last IPS. **a** histological images of the lung tissues; **b** number of EHTB per cm^2 lung tissue and **c** Zn^{2+} content in the lung tissues at different time points. *Bars* = 50 μm

Effects of nZnO particles and $ZnCl_2$ solution on other organs and serum of wild-type rats

Obvious lesions and macrophages containing vacuolar vesicles were not found in other major organs including the liver, kidney, spleen, or brain by histological examination (data not shown). The results of blood cell examination are shown in Table S2: The only changes were increased proportions of monocytes and eosinophils that were rapidly recovered within 2 weeks post exposure. Biochemical

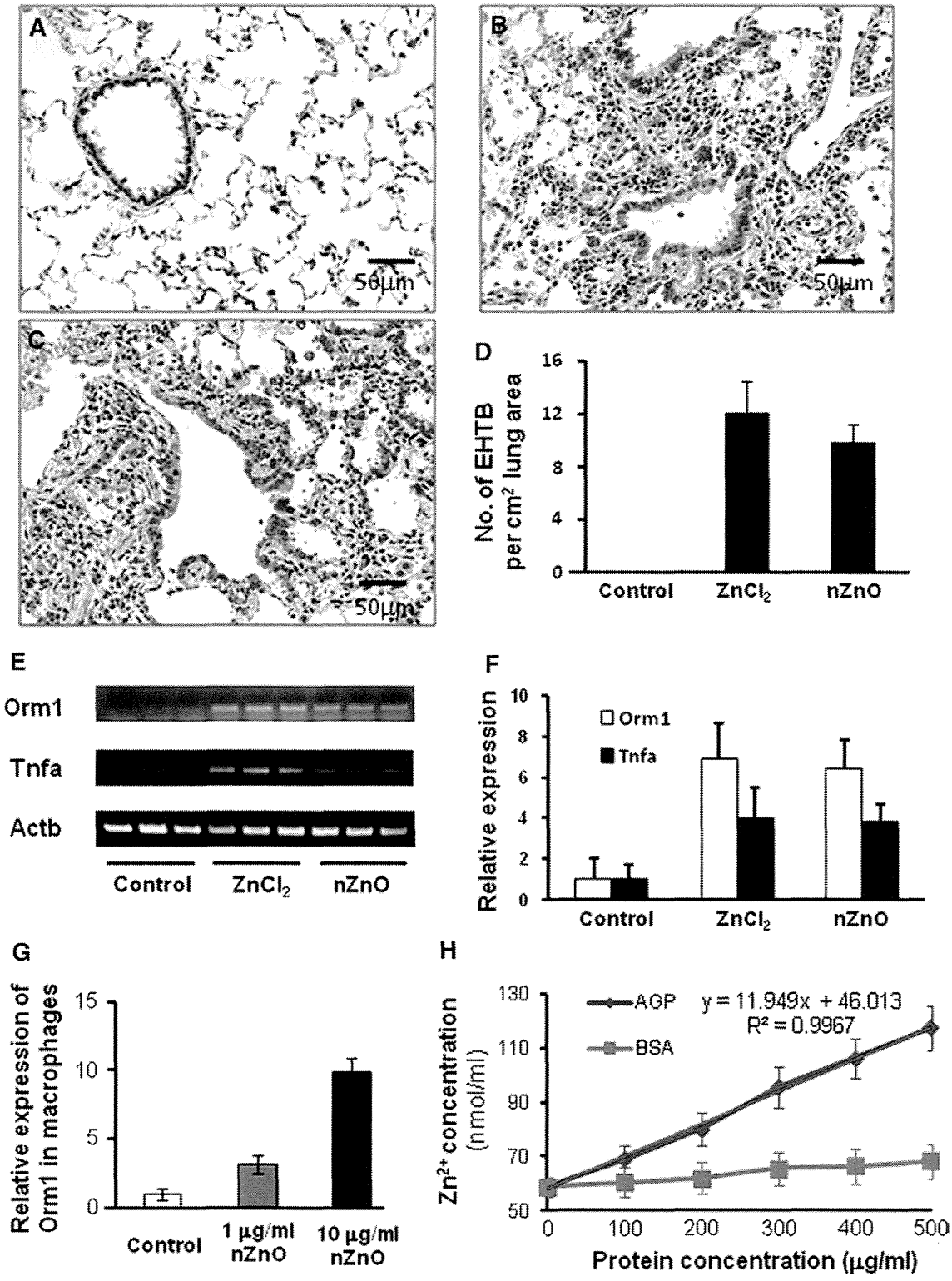

Fig. 4 Similar effects of $ZnCl_2$ solution and nZnO in induction of EHTB and FAIP in wild-type rats. **a** H&E-stained slides of the lungs of rats treated with vehicle; **b** with nZnO; and **c** with $ZnCl_2$ solution, showing EHTB and FAIP; **d** comparable number of EHTB per square centimeter of the lung tissues induced by treatment of $ZnCl_2$ and nZnO; **e** gene expression determined by RT-PCR of Orm1 and Tnfa, with Actb gene as an internal control; **f** real-time PCR analysis of gene expression of Orm1 and Tnfa, which was normalized with Actb expression; **g** induction of Orm1 expression in primary alveolar macrophages exposed to nZnO; and **h** effect of human alpha 1 acid glycoprotein (AGP) and bovine serum albumin (BSA) on dissolution of nZnO in vitro